Renewable and Sustainable Energy Reviews 189 (2024) 113920

Contents lists available at ScienceDirect

Renewable and Sustainable Energy Reviews

journal homepage: www.elsevier.com/locate/rser

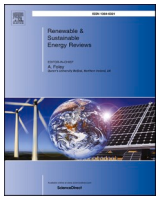

Adaptive systematic optimization of a multi-axis ocean wave energy converter

Alireza Shadmani [a,b], Mohammad Reza Nikoo [c,**], Amir H. Gandomi [d,e,*]

[a] Department of Maritime Engineering, Amirkabir University of Technology, Tehran, Iran
[b] Faculty of Engineering and Architecture, Department of Electromechanical, Systems, And Metal Engineering, Ghent University, Belgium
[c] College of Engineering, Department of Civil and Architectural Engineering, Sultan Qaboos University, Muscat, Oman
[d] Faculty of Engineering & Information Technology, University of Technology Sydney, Ultimo, Australia
[e] University Research and Innovation Center (EKIK), Óbuda University, 1034 Budapest, Hungary

ARTICLE INFO

Keywords:
Ocean wave energy
Wave energy converter
BEM solver
EMnO
Systematic design

ABSTRACT

Due to the growing global energy needs, renewable energy systems, particularly wave energy converters (WECs), are a feasible solution to satisfy current energy demand. Recently, wave farms with diverse technologies, geometries, and layouts have been developed; however, evaluating the performance of these devices is complicated and requires precise hydrodynamic modeling to efficiently deploy wave farms. This study proposes a multi-scenario model using boundary element method (BEM) solver, NEMOH, integrated with evolutionary many-objective algorithms to evaluate the performance of a multi-axis point absorber WEC with respect to cylindrical, triangular, quadrilateral, and octagonal geometries and varying dimensions, that is, radius, draft, and height. To this end, six objective functions were considered to maximize the energy absorption and significant velocity and to minimize the separation distance, levelized cost of energy, net present value, and *q*-factor. Accordingly, three EMnO frameworks were utilized: the non-dominated sorings genetic algorithm (NSGA-III), reference point-based NSGA-III (*R*-NSGA-III), and multi-objective evolutionary algorithm by decomposition (MOEA/D). The results of the three optimization algorithms indicate that *R*-NSGA-III converges faster than the other two and also found that the cylindrical and octagonal geometries produce more annual energy among other forms. Comparing the performances of the three different layouts for cylindrical and octagonal geometries reveals that the arrow layout with thirty buoys produced more energy and had a lower levelized cost of energy and net present value.

1. Introduction

It is vital to develop a more efficient system and manage renewable energy devices to support the large power generation that can be linked to the smart grid. Such a system is affected by the importance of renewable energy, growth of the energy sector, and promising applications of ocean waves. As seen in Fig. 1, the smart grid cannot function without the widespread installation of small electricity producers, specifically WECs. Jin and Greaves [1] explores the UK's advancement in wave energy and the 2050 net-zero objectives, noted by experts to assess wave energy resources, strategic zones, and available data. The authors emphasized accomplishments and the vital involvement of government and industry. It also addressed wave energy's part in decarbonization and necessary future actions. Meanwhile, Guo and Ringwood [2] provide an exploration of wave energy technology and its commercial possibilities. They highlighted obstacles in commercializing wave energy prototypes such as diverse operational principles, deployment alternatives, and a lack of consensus in technology. They mentioned that the slow pace of advancement and business failures have affected investor confidence and also provided an up-to-date survey of the potential of wave energy. Constructing wave farms would enable us to gather more electricity than merely installing individual devices due to the abundance of ocean wave energy compared to other kinds of energy, such as wind, solar, hydropower, etc. In addition, determining the shape and size of WECs for a specific location is another crucial step in gathering more energy. Clemente et al. [3] provided a comprehensive review of WECs, outlining their advantages over other green energy sources such as solar and wind, while also addressing the challenges hindering their commercial success. Their investigation examined technologies

* Corresponding author. Faculty of Engineering & Information Technology, University of Technology Sydney, Ultimo, Australia.
** Corresponding author. College of Engineering, Department of Civil and Architectural Engineering, Sultan Qaboos University, Muscat, Oman.
E-mail addresses: m.reza@squ.edu.om (M.R. Nikoo), gandomi@uts.edu.au (A.H. Gandomi).

https://doi.org/10.1016/j.rser.2023.113920
Received 29 December 2022; Received in revised form 26 September 2023; Accepted 17 October 2023
Available online 7 November 2023

Nomenclature

Abbreviations

AEP	Annual energy production
BEM	Boundary element method
CapEx	Capital expenditure
CFD	Computational fluid dynamics
EMnO	Evolutionary many-objective
GA	Genetic algorithm
LCoE	Levelized cost of energy
MOEA/D	Multi-objective evolutionary algorithm by decomposition
NSGA-III	Non-dominated sorting genetic algorithm v3
NPV	Net present value
OpEx	Operational expenditure
PTO	Power take-off
RAO	Response amplitude operator
RNSGA-III	Reference point-based non-dominated sorting genetic algorithm v3
WEC	Wave energy converter

Symbols

$S(f)$	Wave energy spectrum
f	Wave frequency
H_s	Significant wave height
T_{av}	Mean wave period
T_z	Mean zero-up crossing period
m_2	Second power of wave frequency
ρ	Fluid density
g	Gravity acceleration
E	Overall energy in wave per unit area
$v_g(f)$	Group velocity
P	Level of wave power per unit width in wavefront
$\ddot{\xi}$	WEC displacement
M	Inertia mass
f_h	Hydrodynamic force
f_g	Gravitational force
f_{PTO}	PTO force
f_m	Mooring lines force
f_{add}	Additional force
f_{FK}	Froude-Krylov force
f_d	Diffraction force
f_r	Radiation force
f_{hs}	Hydrostatic force
f_e	Excitation force
v	Particle velocity
μ	Dynamic viscosity
υ	Kinematic viscosity
p	Pressure
z	Depth of the seabed
AEP_y	Wave power plant based on the annual energy production
CF_y	Cash flow at year
L	Total number of years of the project's lifespan
r	Rate of interest
$CapEx_y$	Capital expenditure
$OpEx_y$	Yearly operational expenditure
FIT	Feed-in tariff
$(2s)_s$	Double amplitude motion
$S_{ss}(f)$	Dynamic multi-axis velocity
P_{AEP}	Power in annual energy production
$P_i(H_{m0}, T_{m0})$	Power in each combination of significant wave height and wave period
$J_i(H_{m0}, T_{m0})$	Wave energy flux per wave height and wave period
$\widehat{P}_{AEP}$	Maximum power in annual energy production
q	Analytical hydrodynamic interaction of WECs
P_{array}	Power of the WEC arrays
$P_{individual}$	Power of individual WEC

Units

f	Hz
H_s	m
T_{av}, T_z	S
ρ	kg/m^3
g	ms^{-2}
E	Jm^{-2}
$v_g(f)$	S^2m^{-1}
P	Whm^{-1}
$\ddot{\xi}$	m
M	$kg.m^{-2}$
$f_h, f_g, f_{PTO}, f_m, f_{add}, f_{FK}$	kN
f_d	Wm^{-2}
f_r	Wm^{-2}
f_{hs}	kN
f_e	N/m
v	ms^{-1}
μ	Pa-s
υ	m^2s^{-1}
p	Pa
z	m
AEP_y	$MWhy^{-1}$
CF_y, $OpEx_y$	$US\$y^{-1}$
$CapEx_y$	US$
FIT	$US\$MWh^{-1}$
P_{AEP}	$MWhm^{-1}y^{-1}$

that can complement WECs and highlighted potential applications in both nearshore and offshore specialized markets. The primary objective was to present new perspectives that can facilitate WEC development and successful deployment. To this end, several investigations focused on the development of WECs and designing wave farms considering various aspects.

2. Recent advancements in WEC optimization

Various hydrodynamic models, including BEM solvers like NEMOH [5] and WAMIT [6], are commonly used to assess the performance of individual WEC and wave farms. Babarit and Delhommeau [7] provided a comprehensive overview of NEMOH for accurate evaluation of WEC efficiency and features. Cameron McNatt et al. [8] emphasized the significance of assessing water-wave interactions in offshore renewable energy scenarios and discussed the effects on structural load and performance of devices like wind turbine and WEC arrays. Reikard et al. [9] conducted experiments to forecast wave energy at multiple global locations, incorporating noise distributions to represent sea state variability. Their analysis revealed lower power balancing reserves compared to wind and solar power. Penalba et al. [10] compared NEMOH and WAMIT for modeling WECs, evaluating various stages for common WEC concepts. Furthermore, Sheng et al. [11] compared the performance of NEMOH, hydrodynamic analysis of marine structures, and WAMIT, finding that NEMOH and HAMS provide satisfactory results for basic structures but differ in handling more complex structures.

The placement of WECs in an array affects power absorption due to hydrodynamic interactions. Diffraction and radiation are two phenomena associated with near-field and far-field effects, respectively. Diffraction refers to changes in the incident wave field caused by WECs,

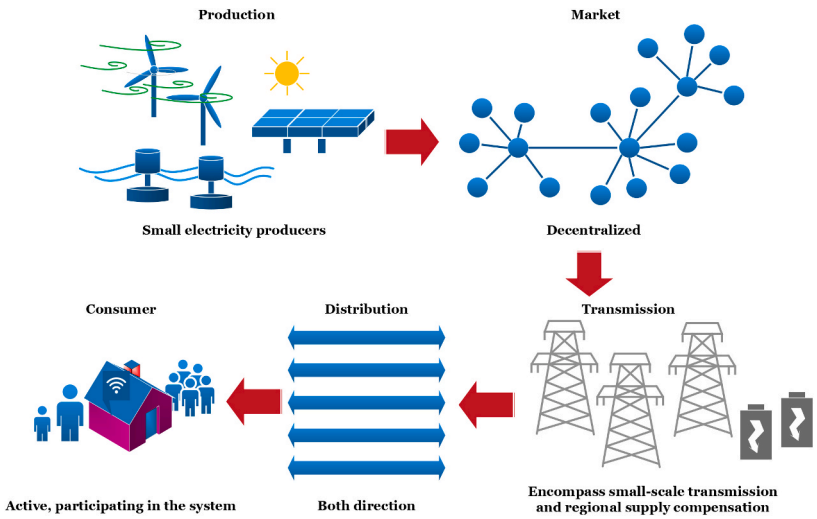

Fig. 1. Future smart-grid flowchart respective to renewable energy serviceability, reproduced from Ref. [4].

while radiation occurs when WECs radiate wave fields due to induced oscillations. Babarit [12] discussed the near-field effect resulting from the interplay of diffracted and radiated wave fields. Marchesi et al. [13] presented a numerical model for a two degree-of-freedom WEC called the energy double system, consisting of a heaving float and a surging paddle with individual power take-off (PTO). Their study involved simulating the system using computational fluid dynamics under experimental conditions.

Reduced wave height due to the wake created by WECs enables them to absorb and redistribute wave energy nearby. This phenomenon, known as the far-field effect, has been extensively studied to optimize array design for maximum power output. Various wave-structure interaction approaches, including computational fluid dynamic (CFD), BEM, and numerical array models with semi-analytical coefficient calculation, have been used to investigate interaction parameters and the near-field effect of WECs. Bozzi et al. [14] studied hydrodynamic interactions among heaving WECs in wave energy parks using a combined hydrodynamic-electromagnetic model and BEM. Verao Fernandez et al. [15,16] developed a methodology that combines MILDwave and NEMOH models to simulate near- and far-field effects of WEC arrays with varying bathymetry. The results demonstrate the suitability of the coupled model for simulating far-field effects under regular and irregular waves. Conversely, Silva et al. [17] evaluated the effectiveness of multiple WEC technologies in the coastal environment of Portugal, assessing their production capabilities at various locations. Various factors, including wave direction, sea states, and overall design, significantly impact the effectiveness of WEC arrays. Optimization techniques are employed to determine the optimal layout for both regular and irregular waves. Teixeira-Duarte et al. [18], Yang et al. [19], and Giassi and Göteman [20] provided comprehensive reviews on the progress of WEC park layout, emphasizing the influence of methodologies, particularly the increasing use of computational intelligence techniques. Loukogeorgaki et al. [21] focused on optimizing linear arrays of heaving WECs near a vertical wall in mild wave environments of the Aegean Sea using a genetic algorithm (GA) coupled with a frequency-domain hydrodynamic model. Their study identified optimum layouts that achieved higher energy absorption, positioning clusters of WECs near the wall edges.

To optimize the interaction between WECs in an array, global optimization is required due to the complex nature of hydrodynamic interaction. Accurate modeling of hydrodynamic interaction is computationally demanding in array optimization. For analyzing the park effect in WEC arrays, moderately fast BEM solvers are recommended to achieve accurate hydrodynamics. However, analytical approximations, like the point absorber approximation, may limit the analysis of more complex array configurations. Lyu et al. [22] used advanced methods to optimize the configuration of various WEC forms, considering device size, geometry, and spacing. Budal [23] introduced the q-factor as a measure of the array's power collection compared to isolated WECs, indicating the impact of interactions on performance. Developed models and an algorithm to optimize the positioning of WEC devices in a wave farm, maximizing performance using the q-factor. Mercade Ruiz et al. [24] proposed an optimization approach for WEC array layouts, considering absorbed power, q-factor, spacing, and deployment area. They compared three optimization algorithms: covariance matrix adaptation evolution strategy, GA, and glowworm swarm optimization, which found that GA and GSO to perform slightly better than CMA-ES with lower computational requirements. Analyzed the interaction and directionality in WEC arrays with optimized oscillating rigid bodies in regular waves. Sarkar et al. [25] utilized a machine learning approach to optimize array layouts, using a statistical emulator and active learning strategy. They employed GA to obtain the optimal layouts for a wave farm with 40 W ECs, considering arbitrary bathymetry and space constraints. Moreover, Shadmani et al. [26] used NSGA-III to optimize the location and layout of wave farms along the coast of Oman, considering maximum annual energy production (AEP) and minimizing q-factors. Sharp and DuPont [27] developed a real-coded GA to optimize the configuration of WEC arrays in a continuous space, considering power and cost objectives. Moreover, Abdulkadir and Abdelkhalik [28] studied the impact of device dimensions on WEC array performance. Comparing heterogenous and homogeneous arrays with equal volumes, they used a dynamic model and optimized control to analyze power output. Through efficient calculation of hydrodynamic coefficients and GA optimization, the heterogeneous array showed a significant performance improvement of up to 40 % in specific wave conditions.

Goggins and Finnegan [29] utilized a GA to optimize the geometric configuration of a WEC structure, aiming to maximize average power extraction at the deployment site. The focus was on devices of different radii to identify the optimal configuration for increased profitability. McCabe [30] used a GA to optimize the shape of a WEC, considering bi-cubic B-spline surfaces and three cost functions. The optimization process involved twelve procedures with varying constraints and penalties on candidate size. Bouali and Larbi [31] developed a sequential optimization procedure for an oscillating water column WEC. Their study examined the impact of PTO model, geometry, and wave directions on device performance using simulations in a numerical wave tank. They identified a single optimal operating point based on factors

such as PTO damping, wall thickness, immersion depth, and wave conditions. Poguluri et al. [32] used an artificial neural network model to optimize WEC rotor design parameters. The ANN considered variables like ballast weight, position, wave frequency, viscosity, and PTO damping to predict mean extracted power. The study involved designing 25 rotor types using linear potential theory and CFD. Ding et al. [33] proposed an integrated cylindrical WEC type breakwater system that optimized performance using CFD and potential flow solver, HAMS. Parametric studies are conducted to improve efficiency, with an additional arc structure significantly enhancing the integrated system. Shadman et al. [34] developed a methodology to optimize the design of a WEC in a nearshore region. By utilizing statistical analysis and hydrodynamic modeling in the frequency-domain, they aimed to maximize power absorption and bandwidth, where design of experiment approach incorporated to obtain the optimized WEC geometry.

Guo et al. [35] examined the current state of geometric optimization in WEC devices, comparing various methodologies and highlighting constraints that hinder future advancements. Moreover, Shadmani et al. [36] reviewed recent trends in the optimal configuration of WECs and emphasized the importance of multi-objective optimization algorithms. Garcia-Teruel et al. [37] optimized WEC geometry to maximize AEP and minimize costs, exploring different definitions and algorithms. Results showed improved objective functions values with adaptable geometry and suitable optimization algorithms. Other studies, such as [38,39], also focused on WEC modeling and geometry optimization. Alamian et al. [40] used multi-objective optimization to optimize a pitch point absorber WEC for the Caspian Sea, by maximizing absorbed power and minimizing construction cost while considering various design shapes. Neary et al. [41] and Previsic and Chozas [42] studied marine energy conversion technologies and their potential impact on the renewable energy market, focusing on the levelized cost of energy (LCoE) in relation to technology performance level and technology readiness level. Additionally, Curto et al. [43] proposed a mathematical model to optimize the energy mix for achieving a fixed percentage of annual electricity production from renewables, considering the LCoE. Piscopo et al. [44] presented a cost-based design procedure for heaving point absorbers, providing recommendations for the design of WEC devices in the Mediterranean Sea. Furthermore, Macadre et al. [45] investigated optimal power aggregation methods for energy converters, considering economic and reliability factors. Their study focused on a case study platform concept combining one wind turbine and twenty WECs to achieve cost savings and risk reduction. Nevertheless, there is no investigation on the optimal configuration of WECs based on the geometry, layout, and economic costs.

While several studies focused on each one of the systematic designs, a minority of recent investigations have considered these factors simultaneously. Kotb et al. [46] focused on enhancing the power output of a Wells turbine for WEC using a CFD-driven response surface amplitude optimization. Through a four-parameter tip modification, the turbine's efficiency was increased, leading to a significant 41.6 % boost in power. Saveca et al. [47] presented a new version of success history-based adaptive multi-objective differential evolution for optimizing the multi-objective WEC problem. This improved version integrates machine learning, particle swarm optimization, and a modified bubble net attaching technique from the Whale optimization algorithm. Through simulations and benchmark tests, the results showed that this new algorithm outperforms recent alternatives, adeptly enhancing WEC designs to boost annual energy yields and reduce energy costs per unit. Lin et al. [48] proposed an approach to optimize the shape of a point absorber buoy to decrease drag from ocean currents while maximizing wave energy capture. The shape of the buoy was outlined using a twelve-parameter parametric model. By employing neural networks, computational time was greatly reduced, sidestepping the need for hydrodynamic equation resolutions in each iteration. Using a GA with several functions, they pinpointed an optimal shape that reduced current drag force by 68.7 % compared to a cylindrical buoy, without compromising the energy capture efficiency from waves. Additionally, Tournant et al. [49] optimized a quayside rectangular WECs design to improve wave energy efficiency and cost-effectiveness. Using rectangular designs enabled validation with a linear potential model, and the CMA-ES evolutionary algorithm was used for optimization. In open sea settings, a flat rectangle with specific dimensions maximized efficiency, with a vertical wall enhancing energy capture. Quayside optimal shapes differed from open sea designs. In regular waves, optimal shapes varied, but in irregular waves, one shape stood out. However, adjusting float width in irregular waves barely affected energy capture. The study of Garcia-Teruel and Forehand [50] emphasized the importance of considering manufacturing and material factors in WEC design optimization. They introduced methods to incorporate manufacturing parameters into the design, yielding WEC shapes specific to certain manufacturing techniques. Comparisons revealed improved manufacturing features in designs with manufacturability constraints. Their methodologies offer a foundation for future WEC designs that prioritize innovative shapes that are also manufacturable. Moreover, Jia et al. [51] initiated a WEC design using a gyroscope for energy capture, which incorporates a vacuum-sealed flywheel to improve energy conversion. They created a dynamic model considering interactions among the floater, gyroscope, and PTO system. Numerical simulations analyzed key parameters like flywheel speed, showing their impact on energy capture. For optimization, they applied an advanced multi-objective evolutionary algorithm by decomposition targeting power conversion. Using the technique for preference by similarity to the ideal solution (TOPSIS) method with entropy weighting, they identified the best design solution, aiming to guide efficient WEC system design and operation.

Accordingly, the success of wave energy largely depends on WEC design and optimization. This study offers an adaptive approach to optimize a multi-axis WEC, aligning with global sustainability and environmental goals. Among global climate challenges, this research underscores the critical need to efficiently tap into the oceans' energy potential. This study proposes a methodology to optimize the layout, shape, size, and economic cost of a wave farm deployed along the coast of Oman. Wave energy calculations and hydrodynamic modeling were performed using NEMOH incorporated in Capytaine [52], Python package. Various shapes (i.e., cylindrical, triangular, quadrilateral, and octagonal) and dimensions (i.e., height, draught, and radius) were considered to compute response amplitude operator (RAO) coefficient and other hydrodynamic coefficients. Subsequently, the economic function and layout design objective were also defined to find the optimal solution for WEC performance in arrays concurrently. Finally, evolutionary many-objective optimization (EMnO) algorithms, including NSGA-III, *R*-NSGA-III, and MOEA/D, based on PyMOO [53] and DEAP [54] Python libraries, were implemented to find the optimal solutions.

The hypothesis considered in this study includes three pre-defined structured arrays and simple geometries to find the optimal configurations. The optimal location and layout, economic model, and geometry objective functions were derived from the mathematical models presented by Shadmani et al. [26], Giassi et al. [55], and Goggins and Finnegan [29], which modifications applied to these models to capture different aspect of the multi-axis WEC. Considering the proposed methodology, the contributions of this research are highlighted below.

- Novel objectives were utilized in this investigation based on the layout, geometry, and economic aspects of WECs.
- The wave climate condition of the coast of Oman was considered with respect to different wave angles to obtain the optimal design for wave farm deployment.
- For the first time, six different objective functions were developed to evaluate the systematic design of WEC.
- To verify the systematic adaptive design of WECs, three EMnOs algorithms were developed and performed to compare several aspects

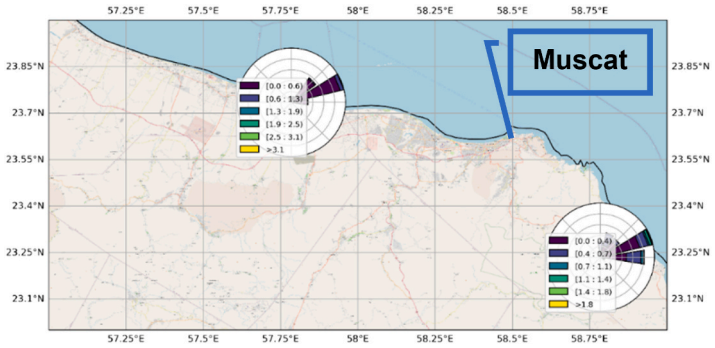

Fig. 2. Wave rose of two stations along the coast of Oman. The left wave rose is for Barka station, and the right is for Quriyat station.

of the device, e.g., hydrodynamic coefficient, layout, geometry, and economic cost.

- The optimal configuration of WECs was obtained by solving the objective functions concurrently.

This research contrasts its findings with a single direction point absorber WEC to identify shared challenges and methodologies across various regions. Although this research centered on multi-axis WECs, the principles can also be relevant to commonly used point absorbers. Using insights from prior studies, a methodology was developed to address current limitations. The study discusses the advantages and disadvantages of current WEC technologies and justifies the chosen analysis method's benefits over traditional techniques. While this research is region-specific, the utilized method can be adjusted for diverse wave climates.

The rest of this study is structured as follows. Section 3 discusses the methodology used in this research, which includes wave energy resources, hydrodynamic modeling and forces, eave farm design, and the developed economic model. Section 4 describes the proposed optimization algorithms and the developed objective functions for this study. Section 5 discusses the results of this research by presenting the optimal geometry design and layout of WECs. Finally, Section 6 concludes the research.

3. Materials and methods

In this section, the research methodology is presented, encompassing various aspects related to wave energy resource assessment and WEC simulation. It covers details about the wave scatter data, power matrix, and the hydrodynamic equations that govern the WEC process. The economic model used in this study is also described. Furthermore, the section provides a comprehensive explanation of the objective functions developed for the study, along with a thorough description of the optimization algorithms utilized.

3.1. Wave energy resources

The wave energy spectrum, $S(f)$, is the approach that is most often used to describe the energy in natural sea waves. It specifically shows how the wave energy at a certain point varies with wave frequency, f, which gives a precise insight into the energy distribution over a specific period since the sea state at a particular point is continually changing. The significant wave height, H_s and mean wave period, T_{av}, are the two key factors to characterize the wave climate of a particular spot. Significant wave height is determined by integrating the wave energy spectrum, $4\sqrt{\int_0^\infty S(f)df}$. The mean wave period and wave energy spectrum are calculated by the mean zero up-crossing period, T_z, so that $T_{av} = 1.09\sqrt{m_0/m_2}$, where m_2 is the second power of wave frequency in the wave energy spectrum.

Lastly, the overall energy in a wave per unit area in terms of H_s and

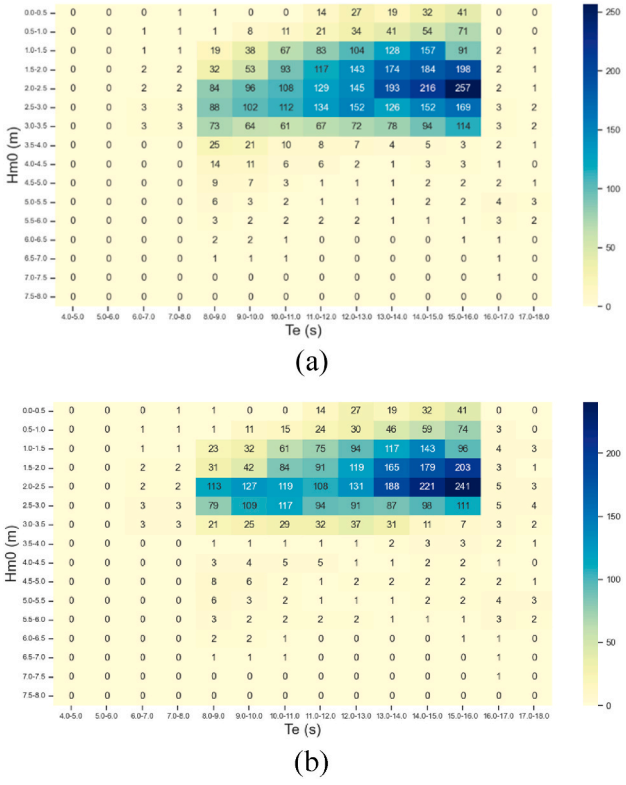

Fig. 3. Probability of occurrence of sea states along the coast of Oman: (a) Barka and (b) Quriyat stations.

m_0 is defined as follows [56]:

$$E = \rho g \int_0^\infty S(f)df = \frac{\rho g H_s^2}{16} \tag{1}$$

where ρ is the fluid density and g is the gravity acceleration. Accordingly, the level of wave power per unit width in a wavefront is measurable using the group velocity in deep waters, where $v_g(f) = \frac{g}{4\pi f} = \frac{gT_{av}}{4\pi}$, as follows:

$$P = \rho g \int_0^\infty v_g(f)S(f)df = \frac{\rho g^2 H_s^2 T_{av}}{64\pi} \tag{2}$$

The wave resource and direction along the coast of Oman are displayed in Fig. 2 in terms of wave rose, in which only two stations' wave data were available. Moreover, the wave energy resource at these two

Table 1
Comparison of Navier-Stokes equation and potential flow theory.

Navier-Stokes equation compressible	Navier-Stokes equation incompressible
$\frac{\partial \rho}{\partial t} + \nabla.(\rho v) = 0$ $\frac{\partial \rho v}{\partial t} + \nabla.(\rho v \otimes v) = -\nabla p + \mu \nabla^2 v + \rho g$	$\nabla.v = 0$ $\frac{\partial v}{\partial t} + \nabla.(v \otimes v) = -\frac{1}{\rho}\nabla p + \nu \nabla^2 v + g$
Nonlinear potential flow	**Linear potential flow**
$\nabla^2 \varphi = 0$ $\frac{\partial \varphi}{\partial t} + \frac{(\nabla \varphi)^2}{2} + \frac{p}{\rho} + gz = C$	$\nabla^2 \varphi = 0$ $\frac{\partial \varphi}{\partial t} + \frac{p}{\rho} + gz = C$

stations was measured respective to the probability of occurrence of each sea state, as shown in Fig. 3.

3.2. Hydrodynamic modeling and forces

The hydrodynamic model plays a crucial role in WEC design and optimization as it significantly impacts the optimal configuration. Similarly, PTO modeling and parameter tuning are essential factors in WEC configuration. While the hydrodynamic model requires careful consideration for trade-offs between computing practicability and modeling accuracy, the PTO model is comparatively simpler due to fewer alternatives and uncertainties [57]. The dynamics of a point absorber WEC are described below.

The dynamics of a point absorber are demonstrated using a floating cylinder. Newton's second law outlines the regulations that a motion of body must follow, as expressed in Eq. (3):

$$\boldsymbol{M}\ddot{\xi}(t) = \boldsymbol{f}_h(t) + \boldsymbol{f}_g(t) + \boldsymbol{f}_{pto}(t) + \boldsymbol{f}_m(t) + \boldsymbol{f}_{add}(t), \tag{3}$$

where WEC displacement is denoted by ξ; and $\boldsymbol{M}$ is the inertial matrix. The hydrodynamic, gravitational, PTO, and mooring line forces are denoted as $\boldsymbol{f}_h.\boldsymbol{f}_g.\boldsymbol{f}_{pto}$ and $\boldsymbol{f}_m$, respectively. The term $\boldsymbol{f}_{add}$ is used to describe additional forces, such as those brought on by safety strategies. The magnitude of each of these elements corresponds to the number of WEC objects and degrees of freedom considered. A WEC body can move in six degrees of freedom: surge, sway, heave, roll, pitch, and yaw. For the movements in pitch, roll, and yaw, torque expressions are employed in place of the corresponding components of the force vector [58,59].

The hydrodynamic force $\boldsymbol{f}_h$ is comprised of several elements: the Froud-Krylov force $\boldsymbol{f}_{FK}$, diffraction force $\boldsymbol{f}_d$, radiation $\boldsymbol{f}_r$, and hydrostatic force $\boldsymbol{f}_{hs}$. Each of these forces is defined by its own particular equation:

$$\boldsymbol{f}_h = \boldsymbol{f}_{FK} + \boldsymbol{f}_d + \boldsymbol{f}_r + \boldsymbol{f}_{hs} \tag{4}$$

$$\boldsymbol{f}_{FK} = \rho \iint_S \frac{\partial \varphi_i}{\partial t} \boldsymbol{n}_h dS \tag{5}$$

$$\boldsymbol{f}_d = \rho \iint_S \frac{\partial \varphi_d}{\partial t} \boldsymbol{n}_h dS \tag{6}$$

$$\boldsymbol{f}_r = \rho \iint_S \frac{\partial \varphi_r}{\partial t} \boldsymbol{n}_h dS \tag{7}$$

$$\boldsymbol{f}_{hs} = \rho \iint_S gz \boldsymbol{n}_h dS \tag{8}$$

It is important to remember that while a WEC object is floating and motionless in the water, the excitation force is defined as $\boldsymbol{f}_e = \boldsymbol{f}_{FK} + \boldsymbol{f}_d$ and $\boldsymbol{f}_{hs} + \boldsymbol{f}_g = 0$. When there is an imbalance between buoyancy and gravity, the hydrostatic pressure applies a balancing force in the heave, roll, and pitch directions when the structure deviates from equilibrium. For linear incident waves, it is common to find an analytical solution. However, for certain standard WEC shapes such as spheres and cylinders, analytical solutions for φ_d and φ_r [60]. Since it is difficult to analytically solve φ_d and φ_r for different WEC shapes, BEMs are most often utilized to provide numerical estimates of φ_d and φ_r. For instance, WAMIT, NEMOH, AQWA, AQUA+, and WADAM are all significant BEM solvers for calculating the frequency-domain response. For the time-domain response, ACHILD3D is the standout [12,36,56].

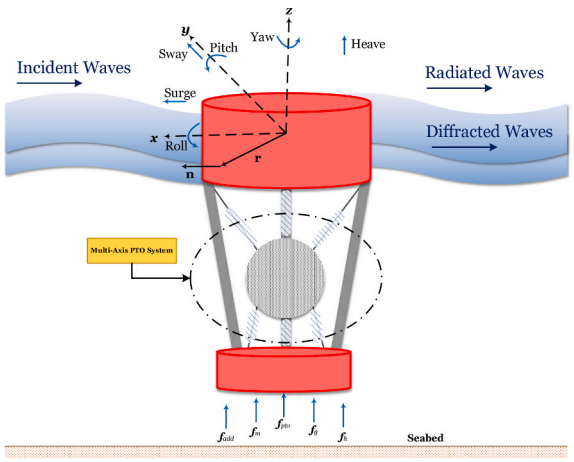

Fig. 4. Schematic view of multi-axis WEC and potential DOF of a floating structure.

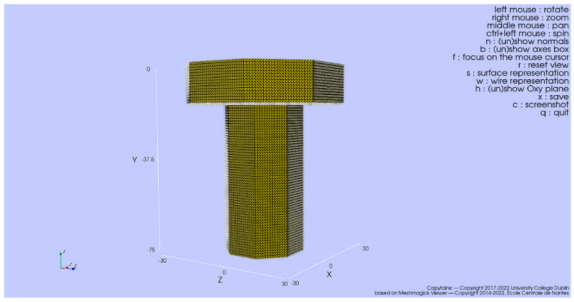

Fig. 5. Initial dimensions of multi-axis WEC.

The pressure layout within a fluid is typically acquired by numerical solutions to either the Navier-Stokes equations or the Laplace and Bernoulli equations. CFD for Navier-Stokes equations and potential flow theory for the Laplace and Bernoulli equations are the two primary methods for solving these equations [35]. Table 1 shows how the Navier-Stokes equations may be reduced to the Laplace and nonlinear Bernoulli equations under the presumption of an ideal fluid, i.e., incompressible, inviscid, and irrotational flow.

The movement of a WEC in response to wave excitation follows Newton's second law, but in a linear dynamic system, this motion can be analyzed in the frequency domain. The BEM solver NEMOH is used to calculate hydrodynamic coefficients and excitation forces, providing insights into the hydrodynamic characteristics of the WEC structure [61,62]. A linear damper model represents the PTO system, assuming a constant PTO damping factor (b_1). This model is compatible with frequency-domain solutions and is used to evaluate the dynamic response. RAO can be determined based on the equation of motion, considering the excitation force and wave amplitude.

3.3. A multi-axis WEC mechanism

It is clear that most point absorber WECs produce energy only from a single direction. For this purpose, a multi-axis point absorber WEC incorporating a heavy ball is assumed to generate energy from multiple axes. Aggidis and Taylor [62] conducted preliminary experiments on this innovative and particular form of WEC. The heavy ball and PTO mechanism can be easily seen from the cut-off in the design of the

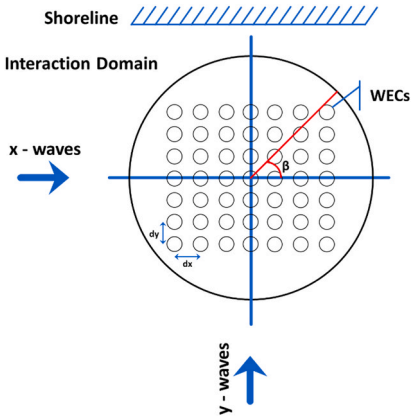

Fig. 6. Sketch of WECs within the interaction domain for the simulation of layouts.

Table 2
Economical model variables.

Economical Model	**Capital Cost (CapEx)**	Cost of the Device ($CapEx_{WEC}$)	Cost of the buoy (C_{buoy})
			Cost of the casing (C_{casing})
			Cost of the foundation ($C_{foundation}$)
			Cost of the stator (C_{stator})
			Cost of the translator ($C_{translator}$)
			Cost of the labor (C_{labor})
			Cost of the extra material ($C_{extra-material}$)
		Cost of the Electrical System ($CapEx_{ES}$)	Cost of the cables ($CapEx_{cables}$)
			Cost of the substation ($CapEx_{SS}$)
		Cost of the Installation ($CapEx_{Inst}$)	Cost of the WEC Installation ($CapEx_{Inst-WEC}$)
			Cost of the electrical system ($CapEx_{ES}$)
		Cost of the Decommissioning ($CapEx_{Dec}$)	Cost of the WEC Installation ($CapEx_{Inst-WEC}$)
			Cost of the electrical system ($CapEx_{ES}$)
	Operation Cost (OpEx)	Cost of the annual repair of the buoy ($OpEx_{r-Buoy,y}$)	
		Cost of the annual repair of the generator ($OpEx_{r-Gen,y}$)	
		Insurance Cost ($C_{insurance,y}$)	
	Levelized Cost of Energy (LCoE)	Capital cost (CapEx)	
		Operational Cost (OpEx)	
		Net Present Value (NPV)	

multi-axis WEC, shown in Fig. 4. The main advantage of the multi-axis WEC is that it can absorb energy from multiple directions. Thus, the hull shape used in this study is based on the TALOS-II design, which was created with a triangle chamfered edge section. Fig. 5 shows the overall dimensions of the original geometry.

3.4. Wave farm design

Wave farm design involves optimizing the layout of multiple WECs, anchoring, mooring, electrical infrastructure, and adaptive control systems, all while considering the unpredictable ocean environment and ensuring long-term reliability. The project cost is significantly influenced by the number of WECs, warranting its consideration in optimization. To ensure the array layout does not become overly expansive, deployment is confined to a specific region. This approach simplifies lease area implementation for the wave energy project [63]. Constraints on WEC separation and the *q*-factor further ensure the layout does not become overly dense. With respect to hydrodynamical interactions between the buoys, two approaches can be followed: (i) semi-analytical approach such as the point-absorber approximation and (ii) numerical methods. The point absorber approach assumes buoys are sufficiently small, leading to non-scattered wave interactions only [64]. This is valid for larger separation and lower frequencies. While increasing structures can magnify errors, it also lengthens simulation times, inhibiting full interaction analysis. In the numerical methods, such as NEMOH, complete hydrodynamical interactions are incorporated. Therefore, this numerical approach can validate the approximate analytical procedure [24,28].

This research aimed to design wave farms using structured layouts, set in rows and columns, with WECs positioned based on interactions, as depicted in Fig. 6. Layouts can be described using various parameters such as row spacing, column spacing, row angles relative to the *x*-axis, and the angle between rows and columns. The *x*-axis is presumed to align with the primary wave propagation direction, while the *y*-axis stands perpendicular to *x*. When considering wave directionality for sea state depiction, the primary direction with the highest likelihood is selected. Further details about the structure of arrays are discussed in Section 4.4.

3.5. Economic model

Here, an economic model, introduced by Giassi et al. [55], is offered to calculate the capital expenditure (CapEx), operational cost or expenditure (OpEx), NPV, and LCoE. Each sub-variable of these parameters is illustrated and described in Table 2.

The inputs required consist of details about the buoy and park, the power output of the platform or park, the efficiency of the WEC conversion, project lifespan, the distance between the installation site and the shore, interest rate, and feed-in tariff. Additional information regarding these parameters can be found in Ref. [55].

The yearly income, cash flow, payback time, NPV, and LCoE are computed once CapEx and OpEx have been estimated. For a designated number of WECs and a constant configuration, the annual income (US$) is always similar to the annual park output multiplied by the feed-in tariff. The result of deducting yearly OpEx from yearly income is known as the CF_y. The payback time is the number of years that must elapse until the cumulative cash flow is positive. Efficiency assessments, including those of wave power plants, may make use of the NPV, which is determined as follows:

$$NPV = \sum_{y=0}^{L} \frac{CF_y}{(1+r)^y} = -CapEx + \sum_{y=1}^{L} \frac{AEP_y.FIT - OpEx_y}{(1+r)^y} \quad (9)$$

where AEP_y is wave power plant based on the annual energy production (MWh/y); CF_y is the cash flow at year (US$/y); L is the total number of years of the project's lifespan; r is the rate of interest; CapEx is the capital expenditure (US$); $OpEx_y$ is the operational expenditure (US $/y); and FIT is the feed-in tariff (US$/MWh), which is frequently subsidized to support initiatives using renewable energy. To guarantee that the venture is successful, the NPV should be positive.

The ultimate goal of the economic model is to compute the LCoE [US $/MWh]. This is determined by dividing the current value of the wave

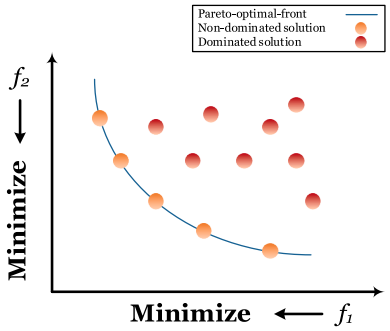

Fig. 7. Non-dominated sorting of a population based on Pareto-front [70].

energy farm's expenses by the electricity output, adhering to Eq. (9), thereby producing the LCoE, expressed as follows:

$$LCoE = \frac{CapEx + \sum_{y=1}^{L} \frac{OpEx_y}{(1+r)^y}}{\sum_{y=1}^{L} \frac{AEP_y}{(1+r)^y}} \tag{10}$$

This metric displays the minimum cost of generated power, which should be sold to break even during the project. This makes it the most often utilized metric for comparing various power production techniques. Throughout this research, the rate of interest and FIT were considered constant, and no inflation was provided.

4. Evolutionary many-objective optimization algorithms

Optimization algorithms aim to find a set of non-comparable solutions called the Pareto-front, representing the trade-off between multiple objectives [65]. While two- and three-objective problems can be graphically represented, many-objective problems typically involve four or more objectives. Most existing techniques focus on one to three objectives, but there is no explicit limit on the number of objectives [66]. To address this, algorithms such as NSGA-III, *R*-NSGA-III, MOEA/D, and multi-objective particle swarm optimization have been developed to find optimal solutions for problems with many objectives. These algorithms expand the capabilities of multi-objective optimization beyond three objectives. Generic EMnO techniques have limitations as they treat multi-objective problems as "black boxes" without utilizing problem-specific knowledge. This can lead to inefficient search queries and detrimental mate selection, impacting the final solution's performance [67]. In this context, three EMnOs are discussed in the following sections.

4.1. NSGA-III

NSGA-III is an extension of the NSGA-II algorithm that can handle a larger number of objectives, typically ranging from four to fifteen. It introduces the concept of reference points to guide the selection process and maintain population diversity. By providing benchmarks, NSGA-III ensures a balanced representation of solutions across the objectives [68]. The fundamental principles of NSGA-III are described as follows [69].

- Highlights non-dominated sorting relying on optimum Pareto fronts, as seen in Fig. 7; exhibits various optimum solutions in each front group between two goals; and works to acquire several Pareto optimum solutions in the examination cycle.
- Utilizes a system designed to maintain variety.
- Compares crowding distances and selects the solutions with the highest score for solutions in the last member of the level (last front F_L).

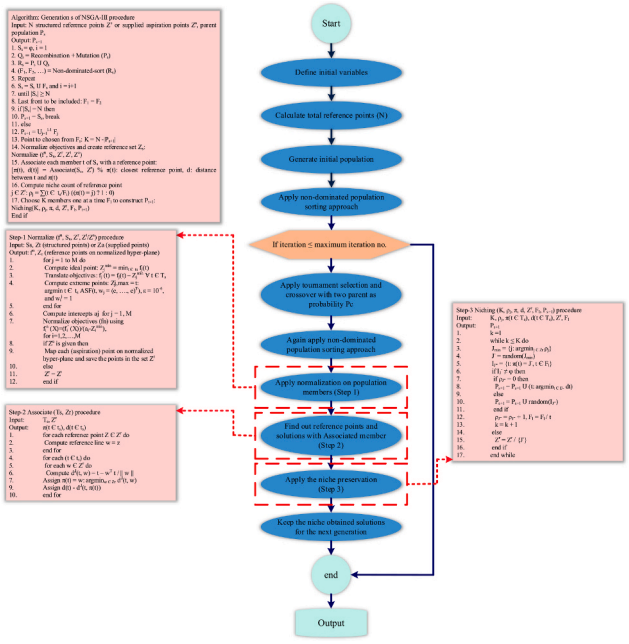

Fig. 8. NSGA-III pseudo-code.

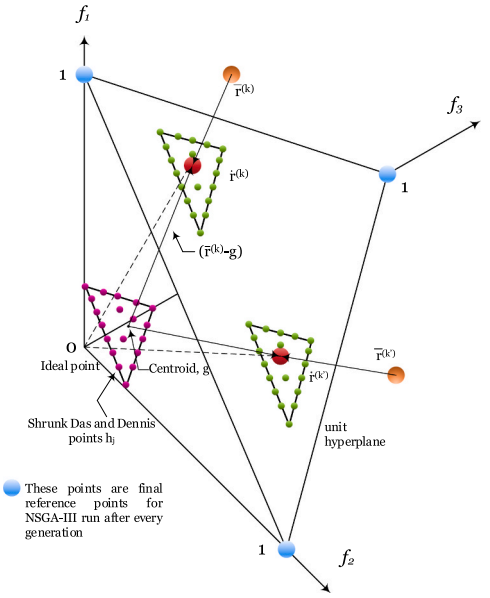

Fig. 9. An illustration of the reference point Z^a calculation process for the *R*-NSGA-III, adopted from Vesikar et al. [71].

- Utilizes the elitism idea of passing on favorable characteristics from one cycle to the next.

Even though NSGA-II has computational complexity $O(mN^2)$, most optimization methods exhibit a complexity of the algorithm of $O(mN^3)$, where m denotes the number of objectives and N is the population size.

The pseudo-code and general algorithm of NSGA-III is presented in Fig. 8.

4.2. R-NSGA-III

The reference point-based NSGA-II (*R*-NSGA-II) was introduced by Deb et al. [68] to address two- and three-objective optimization problems. To further enhance its capabilities, *R*-NSGA-III was proposed by

Algorithm 2: The MOEA/D general framework

Input:
- MOP
- The number of the sub-problems considered in MOEA/D, N
- a uniform spread of N weight vectors: $\lambda^1, \ldots, \lambda^N$
- the number of the weight vectors in the neighborhood of each weight vector, T
- the maximum number of number generations, gen_{max}

Output:
- EP

Step 0 – Setup:
- Set EP = ∅
- $gen = 0$

Step 1 – Initialization
- Uniformly randomly generate an initial internal population, $IP_0 = \{x^1, \ldots, x^N\}$ and set $FV^i = F(x^i)$.
- Initialize $z = (z_1, \ldots, z_n)^T$ by a problem-specific method.
- Compute the Euclidean distances between any two weight vectors and then work out the T closest weight vectors to each weight vector. $\forall i = 1, \ldots, N$, set $B(i) = \{i_1, \ldots, i_T\}$, where $\lambda^{i_1}, \ldots, \lambda^{i_T}$ are the T closest weight vectors to λ^i.

Step 2 – Update: For $i = 1, \ldots, N$
- Genetic operators: randomly select two indexes k,l from $B(i)$, and then generate a new solution y from x^k and x^l by using genetic operators.
- Update of z, $\forall j = 1, \ldots, n$, if $z_j < f_j(y)$, then set $z_j < f_j(y)$.
- Update of Neighboring Solutions: For each index $j \in B(i)$, if $g^{te}(y|\lambda^j, z) \le g^{te}(x^j|\lambda^j, z'')$, then set $x^j = y$ then $FV^j = F(y^j)$.
- Update of EP: Remove from EP all the vectors dominated by $F(y)$. Add $F(y)$ to EP if no vector in EP dominate $F(y)$.

Step 3 – Stopping criteria
- If $gen = gen_{max}$, then stop and output EP, otherwise $gen = gen + 1$, go to Step 2.

Fig. 10. MOEA/D pseudo-code.

incorporating reference points to handle multiple objectives [71]. This approach allows for simultaneous exploration of multiple frames of references, similar to NSGA-II. Compared to standard NSGA-III, *R*-NSGA-III is expected to be faster as it focuses on the Pareto-optimal front. The functionality and efficiency of *R*-NSGA-III were demonstrated through solving various problem instances and realistic scenarios with different objectives. This approach offers two key benefits: identifying additional trade-off points and verifying the existence of Pareto-optimal solutions in previously challenging areas.

Fig. 9 Shows the *R*-NSGA-III approach in action for the two input aspirational values ($\bar{r}^{(k)}, \bar{r}^{(k)}$). A projection is made from the points to the center (pointing out the optimal point of the problem). The projected coordinates $\dot{r}^{(k)}$ and $\dot{r}^{(k)}$ mark the point where the line meets the unit hyperplane. The shrinking Das and Dennis point, h_j, is then transferred to the process to identify $\dot{r}^{(k)}$ and $\dot{r}^{(k)}$ by moving via their centroid, g, on the hyperplane. The whole points collection, Z^a, on the unit hyperplane for an NSGA-III run is made up of the M maximal points and H shrunk points. Thus, *R*-NSGA-III stands in need of a population size of:

$$N_{III} = \left\langle \left(M + K \binom{M+p-1}{p}, 2 \right) \right\rangle, \tag{10a}$$

where $\langle \alpha, 2 \rangle$ denotes the lowest positive value divisible by 2 and larger than α.

4.3. MOEA/D

The MOEA/D has a lower processing sophistication at each generation than NSGA-II by decomposing a multi- and many-objective optimization problem into many scalar sub-problems and optimizing them. The salient characteristics of the MOEA/D method, which was first presented in 2007 b y Zhang and Li [72], include.

i. Presents a simple and effective decomposition method for achieving multi-objective evolution in evolutionary computing.
ii. Lower computational burden than that of NSGA-III at each generation because it solves N scalar optimization issues optimally rather than solving the problem. In addition, it has a rapid rate of convergence [73].

Weighted sum, Tchebycheff, and boundary intersection methods are used to decompose a problem into a set of smaller scalar problems. As shown in Fig. 10, the MOEA/D framework can often break down the approximation Pareto-front issue into N scalar sub-problems via the Tchebycheff method.

Table 3
Comparison of three proposed EMnO algorithms with other techniques.

Algorithms	Advantages	Disadvantages
NSGA-III	• Efficient on high-dimensional data • Better diversity and convergence	• Performance may degrade with the increasing number of objectives
RNSGA-III	• Highly scalable • Use of reference points to guide the search towards the Pareto front • Able to obtain a good balance between convergence and diversity • Able to maintain a diverse set of non-dominated solutions while converging to good solutions	• Requires the selection of appropriate reference points • Computationally expensive
MOEA/D	• Highly scalable • Handling many-objective optimization problems • Handling complex problems • Effective decomposition strategy • Able to find a diverse set of non-dominated solutions while converging to good solutions	• May struggle with non-convex and non-smooth Pareto fronts • Requires the use of difficult points, which may be difficult to choose • May converge to sub-optimal solution if the decomposition weight vectors are not properly set
SPEA2	• Can handle a wide range of optimization problems • Good balance between diversity and convergence	• Performance may reduce with more complex or high-dimension problems
HypE	• Directly optimizes the hypervolume metric • No need for additional parameters like ε in ε-dominance	• Struggle in higher dimensional objective spaces
OMOPSO	• Simple and easy to implement • Low computation cost • Able to handle multiple objectives without requiring any weighting or aggregation • Suitable for problems with continuous and discontinuous Pareto fronts	• May converge to sub-optimal solution if the population size and swarm parameters are not properly set • Not suitable for problems with constraints
GDE3	• Effective for continuous problems • Robust in handling numerical difficulties	• May not be as efficient in combinatorial or discrete problems
SMS-EMOA	• Directly optimizes the hypervolume metric • Ensures diversity of solutions	• Computational complexity can grow quickly with the number of objectives

The reason for opting for the many-objective optimization is primarily because WEC design inherently involves multiple conflicting objectives, like maximizing power output often conflicts with minimizing construction cost or environmental impact. Therefore, EMnO algorithms are beneficial to comprehensively explore these trade-offs. In general, advantage and disadvantage of these three algorithms are presented in Table 3 and compared with other algorithms that can handle many-objective problems.

Regarding the comparison provided in Table 3, the NSGA-III, RNSGA-III, and MOEA/D are chosen to solve the many-objective problem in this study, which the following section will discuss the developed objective functions. Previous studies in WEC design optimization often employed single-objective algorithms that do not fully account for the interplay between conflicting goals like cost, layout, and geometry. By utilizing three EMnO algorithms, this research conducts a comparative analysis to validate the robustness and reliability of the optimization results. This multifaceted approach adds a layer of rigor to this study, ensuring that the solutions provided are both optimal and achievable. The adoption of these algorithms provides actionable insights that are not just academically valuable but also industrially relevant; for

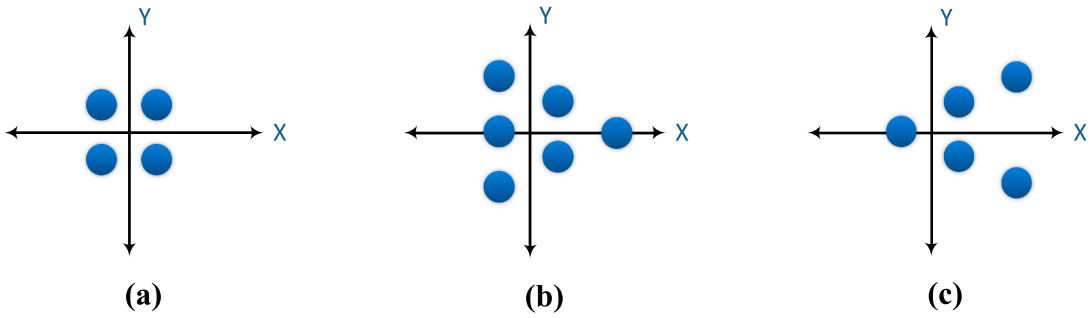

Fig. 11. Default layouts: (a) aligned, (b) staggered, and (c) arrow.

instance, optimized geometry configurations can lead to greater energy output, which directly correlates to increased commercial viability.

4.4. Set-up of adaptive layout – geometry – economic model

There are several design factors or characteristics that must be taken into account to determine the optimal geometry for any given WEC, including (i) the highest wave energy must be effectively captured throughout an appropriate frequency range, (ii) the effectiveness of the converter ought to be unaffected by the wave's orientation, and (iii) slamming must be controlled and reduced if the converter has an extremely dynamic reaction. Considering the previously mentioned factors, the dynamic velocity response of a multi-axis WEC operating in an unconstrained system can be maximized, leading to optimal wave energy extraction. Additionally, when the structure vibrates near its resonance frequency, the multi-axis dynamic response can be substantial enough to warrant consideration of slamming.

There must be an established objective function to evaluate how well each possible geometric arrangement performs. The 'significant velocity,' also known as the 'double amplitude motion,' $(2s)_s$, is the given criterion, which initially introduced by Goggins and Finnegan [29]. The significant velocity is derived based on the energy spectrum similar to the way that the 'significant wave height' is obtained, using Eq. (11):

$$(2s)_s = 4\sqrt{\int_0^{\infty} S_{ss}(f)df} \tag{11}$$

where $S_{ss}(f)$ is the dynamic velocity response. The proposed formula in Ref. [29] only focused on the heave motion of the structure and impose a constraint on the maximum RAO value to prevent slamming. Each structure is evaluated under different RAO values, and the optimal geometric configuration is determined for each constraint. To ensure the stability of the WEC PTO system, a maximum significant wave height of $H_s = 3\ m$ is suggested, where the WEC is not in operation. Stability is also addressed by carefully planning the mass distribution and reducing the meta-centric height to minimize pitch motion. Finally, the formulation in Eq. (11) is modified regarding serviceability in multi-axis motions, namely surge, heave, and pitch. This objective, Eq. (11), aims to maximize the modified significant velocity for the input wave energy spectrum and optimize the geometry configuration.

Various design parameters, including wave energy extraction and shape designs (cylindrical, triangular, quadrilateral, and octagonal), were considered for the optimization of each WEC device. A geometry database was created for the multi-axis WEC, incorporating different radii, heights, and draughts, and shapes. PyMesh [74] was used to generate device mesh, while Capytaine [52] facilitated hydrodynamic modeling using NEMOH. RAO and other hydrodynamic coefficients were calculated based on the device mesh and stored for subsequent optimization processes. Regarding the annual wave energy and economic cost of the multi-axis WEC, a modification was performed on the economic model proposed by Giassi et al. [55] to minimize LCoE. The initial state of LCoE, expressed in Section 3.5, was modified to consider the total cost of the multi-axis WEC device and then minimize it. Therefore, the objective function of the economic process is as follows:

$$f_{cost} = min_q(LCoE^q) \tag{12}$$

where $LCoE^q$ is the levelized cost of energy calculated for each layout; and q is an index of layouts in the population.

In addition to finding the optimum WEC geometry, LCoE, and the ideal optimization problem solution, the q-factor for each arrangement of layouts must be calculated regarding their maximum AEP in the domain. The formulations of optimal placement are given in Eqs. (13) and (14). Additionally, the q-factor was calculated regarding the optimal placement of WEC via Eq. (15):

$$P_{AEP} = argmax\left(\sum_{i=1}^{N} P_i(H_{m0}, T_{m02})\, J_i(H_{m0}, T_{m02})\right)(x_i, y_i) \tag{13}$$

$$\widehat{P}_{AEP} = argmax_{x,y} P_{AEP}(x_i, y_i) \tag{14}$$

$$q = argmax\left(P_{array} \,/\, N * P_{individual}\right) \tag{15}$$

The optimum location and layout of the array were determined within the specified domain using the given equations. The q-factor was optimized for each device placement and array design to achieve the most constructive q values [22]. Simulations were conducted for various wave directions ranging from 0° to 60° with 15° increment allowing for the identification of the best layout design based on calculated q-factors. Hydrodynamic coefficients, including RAO, were computed considering different wave directions and array layouts with 15, 30, and 45 devices. The separation distance between devices in each array was constrained to 25, 50, and 75 m within the domain. The objectives defined in Eqs. (13)–(15) aimed to determine the optimal layout by optimizing the coordinates of WECs (x^i, y^i) to maximize power production and minimize the LCoE value.

WECs in the park are placed on grid nodes measuring 10 m by 10 m to ensure equal area distribution. Each substation has the same number of WECs, determined by three cutoff distances of 25, 50, and 75 m. Radiation and diffraction effects are considered, and power production is calculated for annual sea states. Economic and hydrodynamic models are utilized, minimizing the LCoE through the cost function. The optimal layout is determined by selecting the solution with the lowest LCoE from the Pareto front. Consequently, the optimal layout design is determined by selecting the solution with the lowest LCoE from the Pareto front. Furthermore, the best layout is chosen by taking into account an array with $i = 1, \ldots, n_b$ WECs and a specific number $j = 1, \ldots, n_{ss}$ of offshore stations. This means that each station has a certain number of n_{bc}^j of WECs. Therefore, the cost of the WECs is determined by which of the n_b devices in the entire array will be allocated to the jth station. Consequently, the WECs of the array should be clustered in a way that minimizes the sum of the total distances between the WECs and the station.

Multiple initial points need to be tried to find the global minimum

Table 4
Selection logic and limitations of three pre-defined layouts.

Layout	Selection logic	Limitations
Aligned	oSimple and most intuitive configuration oEnsuring each WEC is exposed to the wavefront uniformly	oIn scenarios where waves have a dominant direction, aligned layout might not make the best use of wave interactions oMay lead to shadowing effect
Staggered	oCan take advantage of wave interactions and interference patterns oCan help capture energy from waves that might have been missed oAllow WECs to benefit from modified wave patterns created by their neighbors	oMight suffer from complex interference patterns that can reduce the efficiency of individual WEC oRequires a more sophisticated positioning system to maintain staggered in real sea conditions
Arrow	oUseful in regions where wave directions are predominant and consistent oCan optimize the WEC positioning with respect to the directionality of wave energy	oIts efficiency can significantly drop in regions with variable wave directions oWaves with directions not aligned with the arrow's orientation result in underutilized layout for many WECs

solution. In this study, 50 different randomly initialized centroids were used to simulate the clustering process iteratively. This approach allows for flexible allocation of elements to clusters without fixed numbers. The goal is to minimize the variance of WECs while maintaining the same total rated power for the park, even if individual stations have different power ratings. If each substation in the park had the same power rating, the park's total rated power would be same, although the individual stations have various power ratings.

On top of the objectives presented, optimization frameworks based on three EMnO algorithms, i.e., NSGA-III [75], *R*-NSGA-III [71], and MOEA/D [72], were implemented. The EMnO frameworks were executed using PyMOO [53] and DEAP [54], Python packages. All simulations were conducted using a PC with 12 CPU cores (Ryzen 9 3900 × 3.80 GHz) and 64 GB RAM. The initial WEC layout is illustrated in Fig. 11, in which three pre-defined layouts namely aligned, staggered, and arrow were considered. Table 4 presented the selection logic and limitations of the three pre-defined layouts. Additionally, the procedure of performing optimization algorithms is presented in Fig. 12. According to the flowchart, the wave energy spectrum is imported as an input and then will be converted to the amplitude domain to process as an input for the NEMOH toolbox. In addition, a geometry database is created and added to the procedure of NEMOH that can calculate RAO, dynamic response, *q*-factor, and LCoE of arrays with respect to each geometry and pre-defined layout. In each scenario, the developed objective functions will be evaluated based on the EMnO algorithms, and if the proper size of arrays with maximum energy production is not satisfied, the next iteration will take place. The entire process will be repeated until the threshold values for each objective function are obtained.

While this analysis utilizes advanced optimization algorithms, computational limits restrict the depth to which certain simulations could be run. For instance, a larger domain could provide a larger wave farm design but would significantly increase computational time and resources. In addition, this study relies on available data for wave patterns, which is inherently historical. The ever-changing climatic conditions could result in different future wave patterns that this model might not fully capture.

5. Results and discussion

In the optimization algorithm of geometry configuration, the two specified variables are: the geometry shape (i.e., cylindrical, triangular, quadrilateral, and octagonal) and dimension of the shapes in terms of radii, height, and draught, from which a geometry database was created. Additionally, each dimension varies between 1 and 35 *m* for radii and 1–18 *m* for height and draught. The annual wave energy spectrum was utilized as input to calculate the RAO of each geometry and subsequently obtain the dynamic multi-axis velocity response spectra and modified 'significant velocity' $(2S)_s$. After examining each shape by calculating the modified 'significant velocity,' the shape with the maximum modified 'significant velocity' can be determined as the optimum size. The optimum geometry configurations are recognized in Fig. 12, where the modified $(2S)_s$ for different radii, heights, and draughts in a cylindrical, triangular, quadrilateral, and octagonal shapes are plotted. Three different EMnO algorithms were employed for each shape and size to compare the results of geometry optimization. It should be noted that despite the restriction imposed on RAO in Goggins and Finnegan [29], this study neglected the RAO restriction due to the multi-axis motions assumption.

According to Fig. 13, the optimum radii were found to be between 26.3 and 32.4 *m* for the four considered shapes. NSGA-III achieved the highest values for cylindrical and octagonal shapes for different radii were at the highest value; however, the maximum radii values for triangular and quadrilateral shapes were obtained by MOEA/D. Regarding height, the maximum values were obtained in the range of 13.4–17.7 *m*, in which cylindrical and octagonal shapes achieved the highest values via MOEA/D and *R*-NSGA-III, respectively. Lastly, the

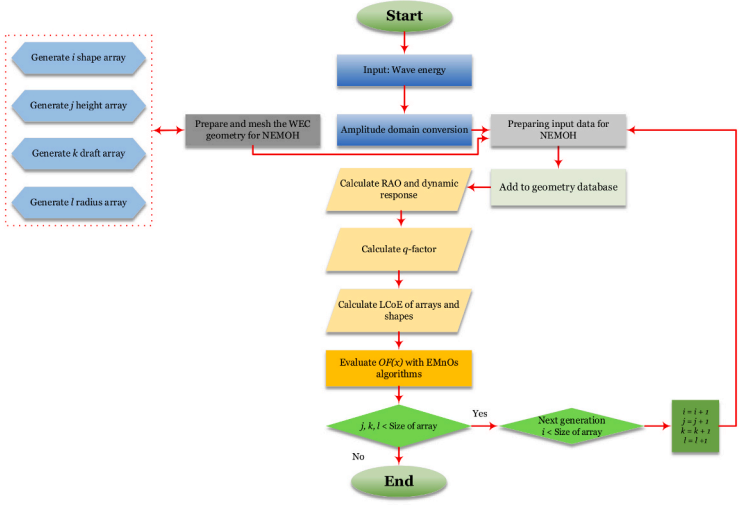

Fig. 12. Flowchart of layout – geometry – economic adaptive design based on EMnOs.

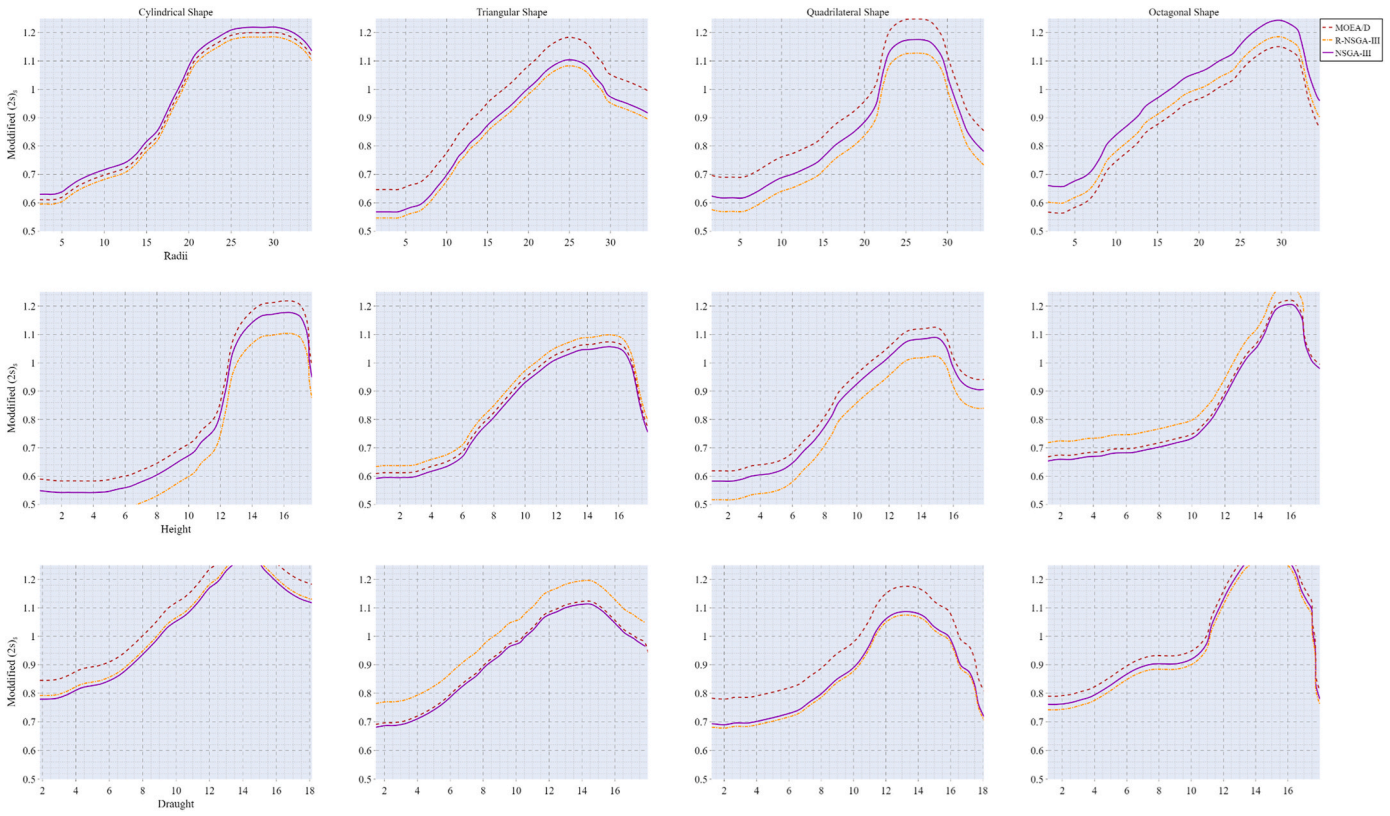

Fig. 13. Modified $(2s)_s$ vs. different sizes of radii, height, and draught.

range of draught for multi-axis WEC was found to be 12.2–17.4 *m*, in which cylindrical and octagonal shapes were at their highest values related to their MOEA/D results. The findings of MOEA/D suggest that the quadrilateral geometry is appropriate up to a radius of 27 *m*. In comparison, the triangular geometry is appropriate for a radius range of 24–28 *m*. Regarding height, it can also be concluded that the quadrilateral height determined by MOEA/D can be used as the optimum geometry. In addition, the triangular geometry reaches its maximum through the *R*-NSGA-III algorithm, which can be an alternative optimum draught for the triangular shape. In addition, the results show that the octagonal shape is optimal, and the cylindrical geometry is nearly optimum with respect to the optimal dimensions, independent of the RAO.

Finally, by comparing the results of each shape and size variation with respect to three different EMnO algorithms, it can be deduced that the cylindrical shape with the derived values of 26.3, 15.2, and 17.2 *m* for radii, height, and draught and octagonal shape with 29, 13.6, and 16.3 *m* for radii, height, and draught, respectively, are the optimal shapes and sizes for the multi-axis WEC to be deployed along the coast of Oman. The results of the EMnOs for the three main dimensions, i.e., radii, height, and draught, against the volume of the four considered shapes are shown in Fig. 14(a)-(d). By changing the obtained WEC radius, height, and draught for cylindrical shape, the absorbed power and volume of the device varied between 1.13 and 1.22 kW and 168–262 m^3, 1.31–1.42 kW and 252–288 m^3, and 1.48–1.57 kW and 163–218 m^3, respectively, as can be seen in Fig. 14(a). It also can be observed that the absorbed power and volume regarding the variation in the optimum dimension for octagonal shape were 1.32–1.39 kW and 150–300 m^3, 1.28–1.33 kW and 284–304 m^3, and 1.29–1.33 kW and 105–254 m^3, respectively. These results are not comparable to triangular and quadrilateral geometries, which had lower AEP_ys, as observed from the Pareto front results of each dimension variation in each shape. By examining the optimization figures, it is clear that many possible configurations are not optimal, demonstrating the importance of geometry optimization for the WEC's usability.

It can be seen in Fig. 14(a)–(d) that increasing the dimensions resulted in more power to be extracted and decreased immersed volume. By comparing the results of these geometries with each other, it can be concluded that cylindrical and octagonal geometries are very effective for increasing the extracted power, which can be impressively enhanced by about 100 Watts.

After obtaining the optimal geometry configuration, the design cost of a WEC must be optimized for deploying multiple WECs. Fig. 15 depicts the LCoE and NPV outcomes of the WEC layout (deployed in aligned, staggered, and arrow layouts at a particular place). For parks with up to 45 W ECs, the LCoE and NPV were estimated for various converter rated powers. The model was run for every sequence of converter power rating and number of WECs. Devices established in the park with increasing WECs match the graphs' significant increases/decreases. Unfavorable results were achieved for a rated power of 20 kW in waves at a 30° angle, while the smallest LCoE was acquired for WECs valued at 100 kW with waves coming from a 45° angle.

By examining the rated power, it can be observed that converters with 100 kW rated power have the best condition with respect to the local wave reproducing and produces the lowest energy costs (or the most significant NPV). Comparatively, lower power ratings result in much less yearly energy output and higher energy costs. Considering the various wave directions, the WECs in the line of the waves coming in (waves with a 45° angle, black lines) drastically varied the results, with up to a 22 % difference respective to parks with 45 W ECs with a rated power of 100 kW. In contrast, the highest LCoE and lowest NPV were obtained for the WECs at shadowing placement, respectively. For 15 and more devices, the LCoE value gradually decreased in layouts without shadowing and increased for layouts with adverse interactions or higher electrical system costs. However, with more than 10 W ECs, the most significant energy cost reduction is possible (a 68 % decrease in LCoE from 1 to 10 W ECs). The value of including the hydrodynamic interaction is shown by contrasting these results with the blue line, wherein hydrodynamic interaction has been omitted. Specifically, results were

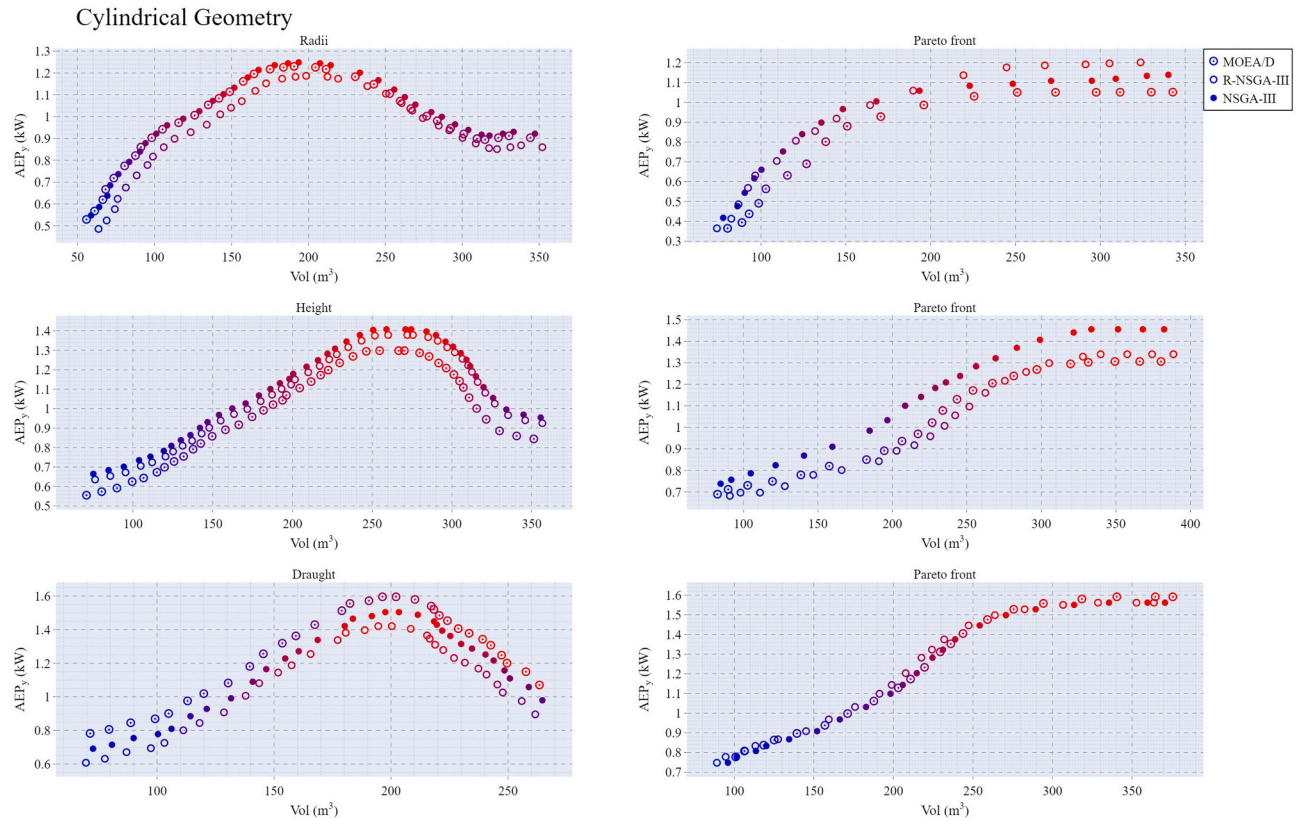

(a)

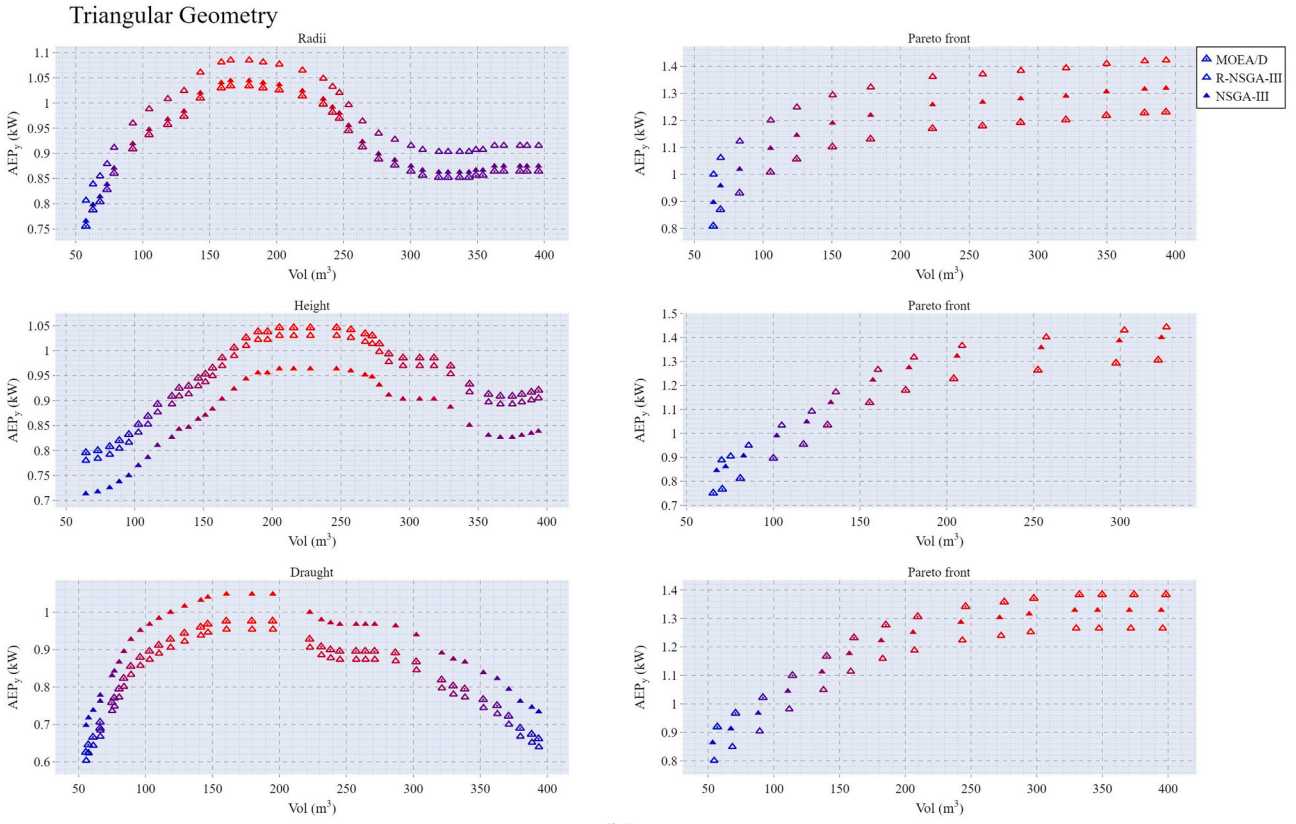

(b)

Fig. 14. AEP$_y$ (left) and Pareto front (right) against the volume of (a) cylindrical, (b) triangular, (c) quadrilateral, and (d) octagonal geometries.

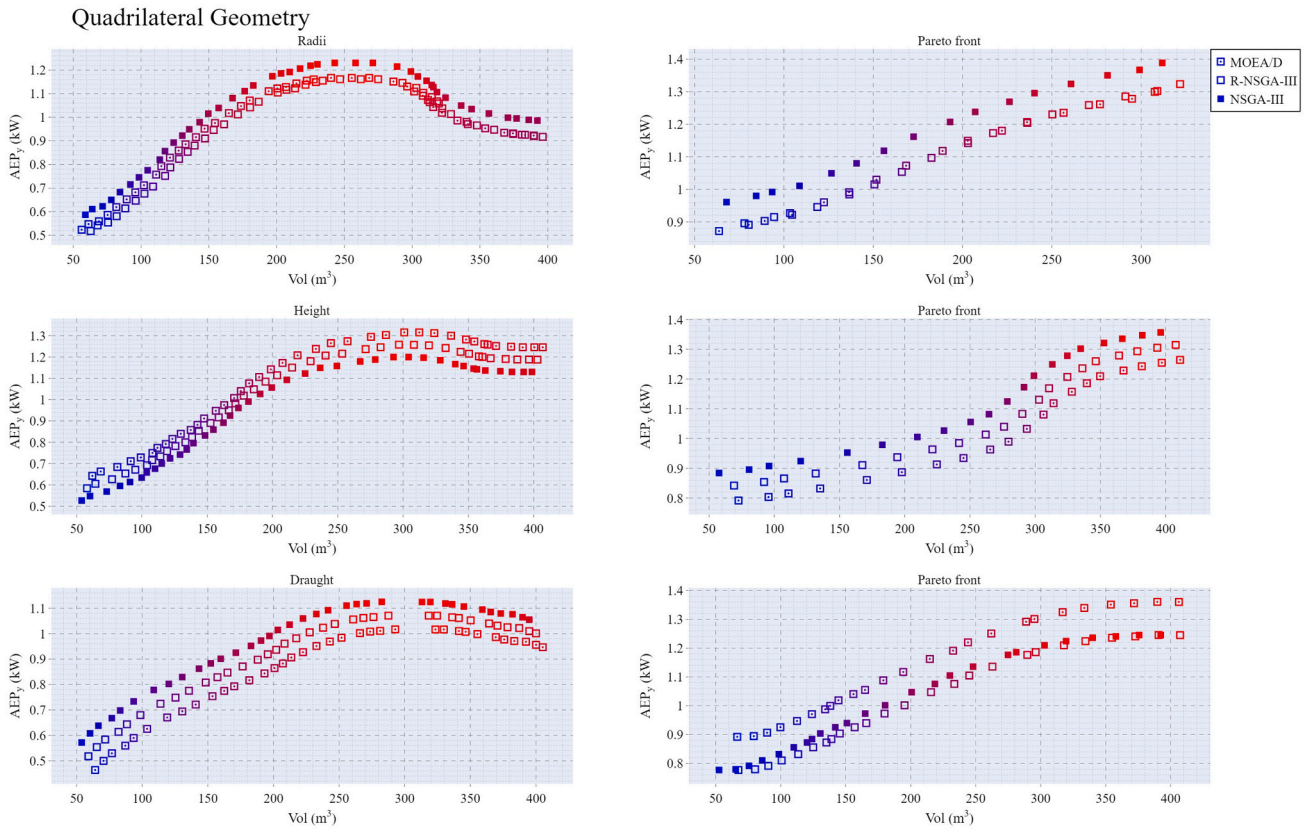

(c)

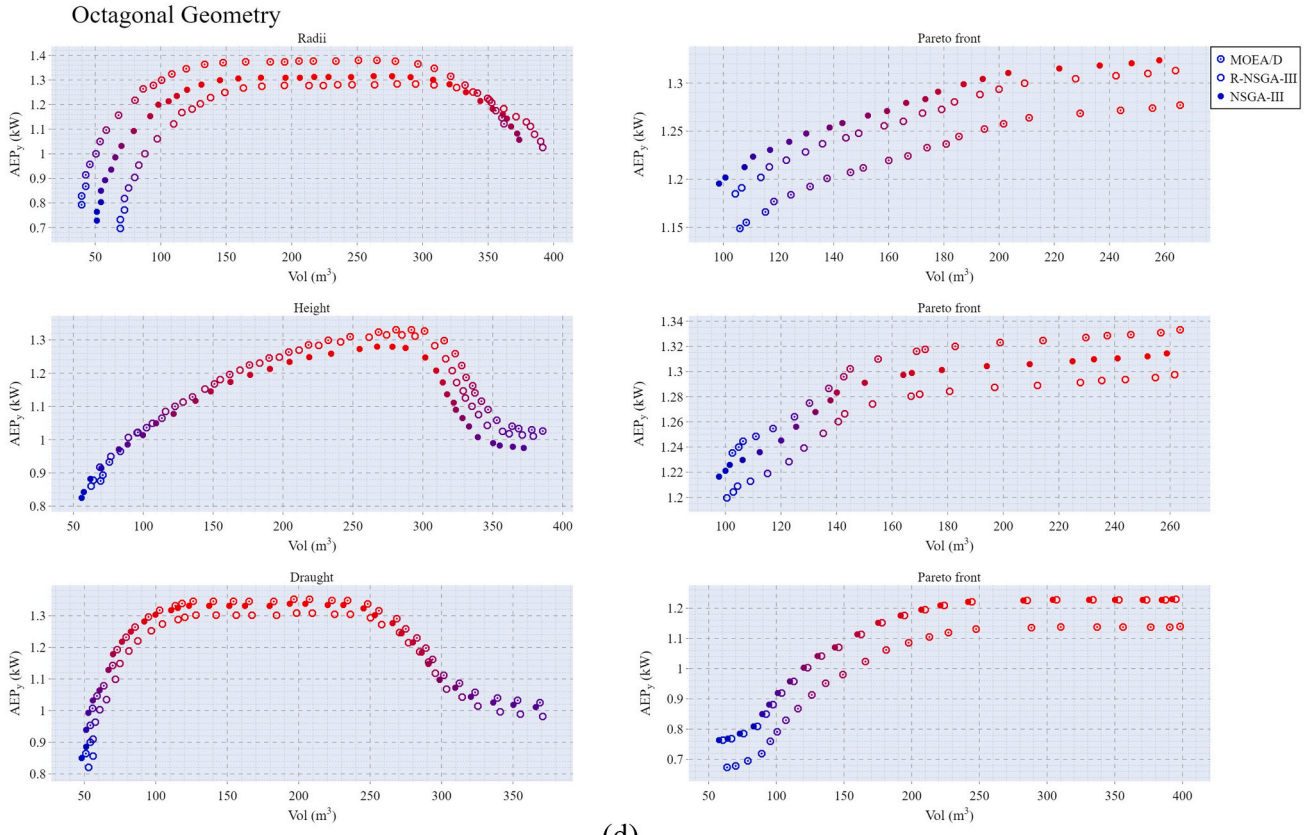

(d)

Fig. 14. (*continued*).

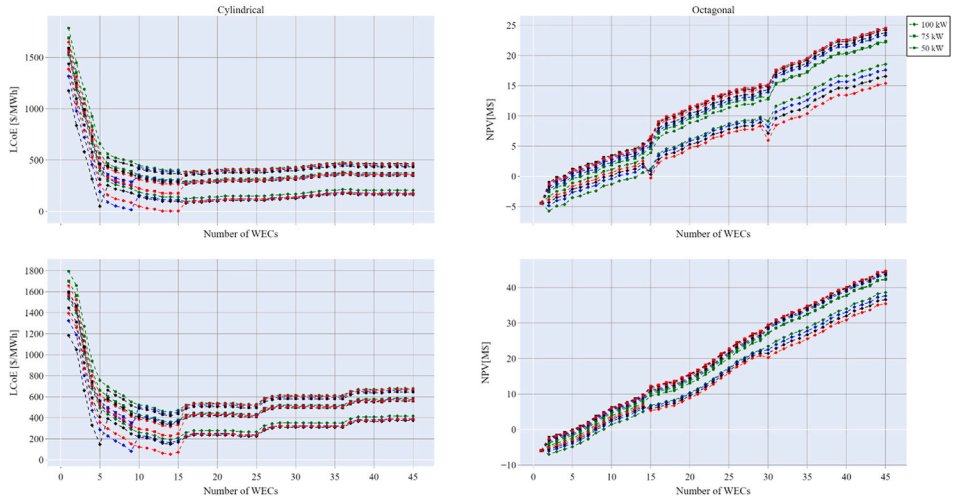

(a)

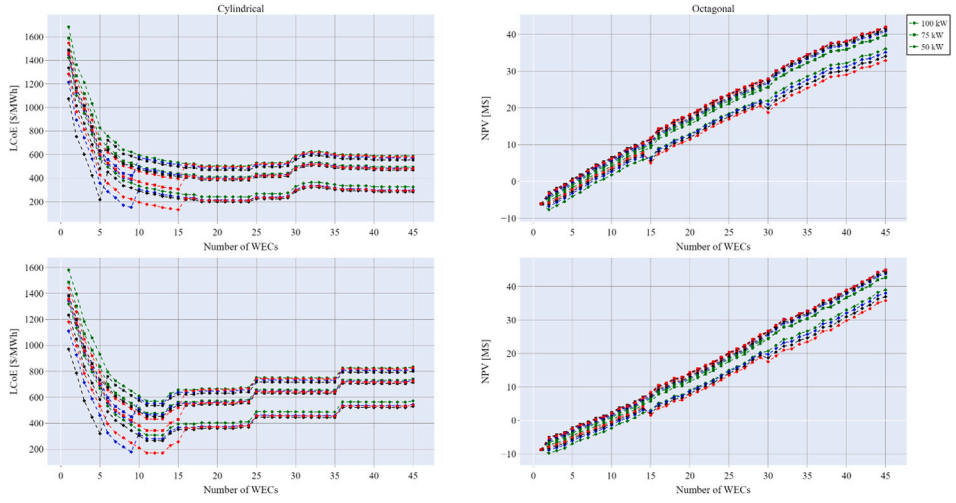

(b)

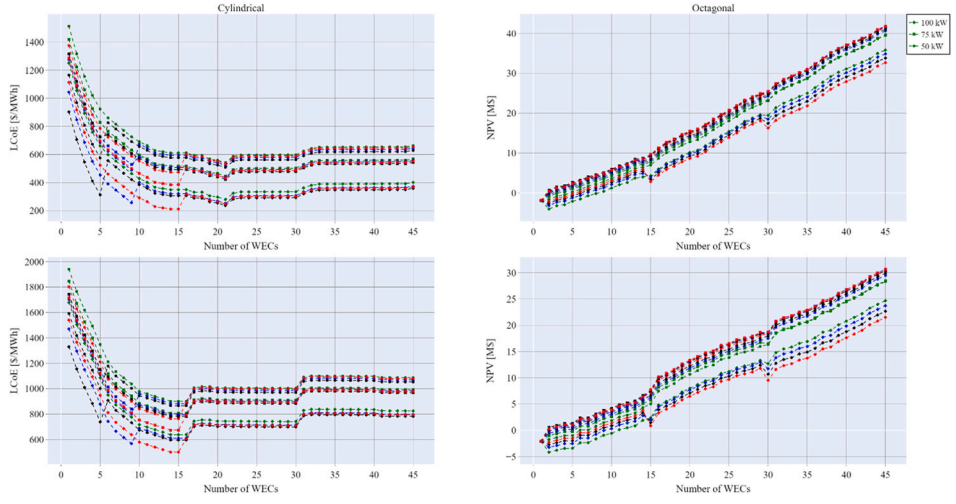

(c)

Fig. 15. LCoE and NPV values vs. number of WECs for optimal cylindrical and octagonal shape with (a) NSGA-III, (b) *R*-NSGA-III, and (c) MOEA/D algorithms.

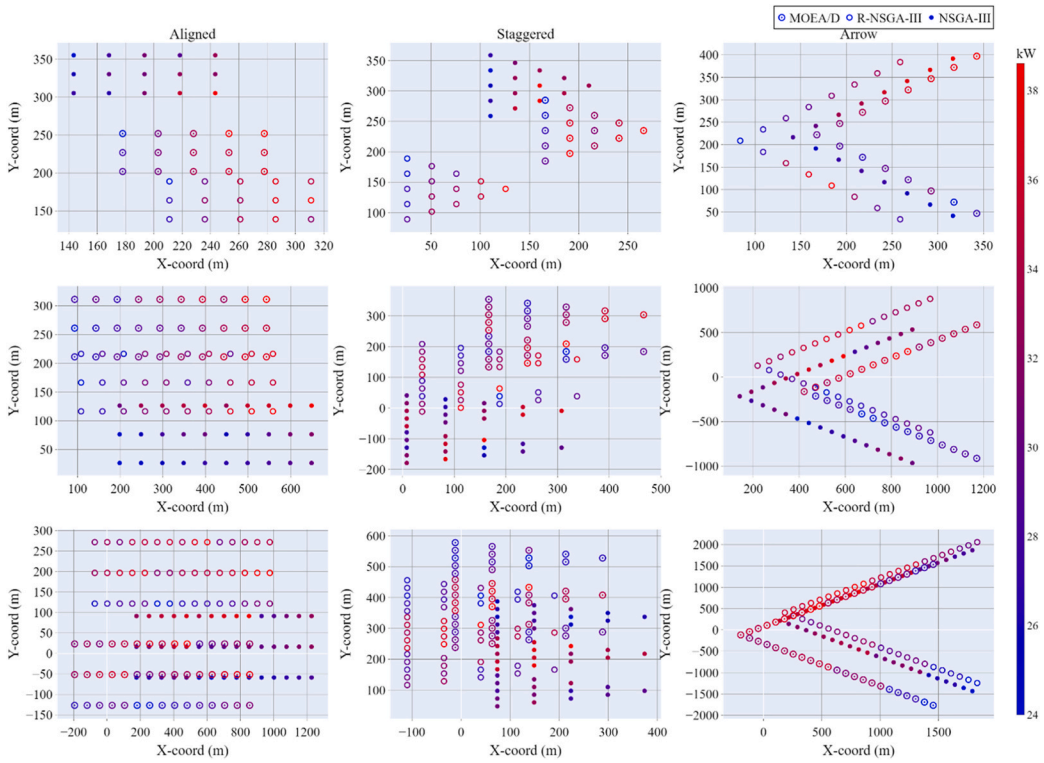

Fig. 16. Layout design of cylindrical WEC with 15, 30, and 45 device.

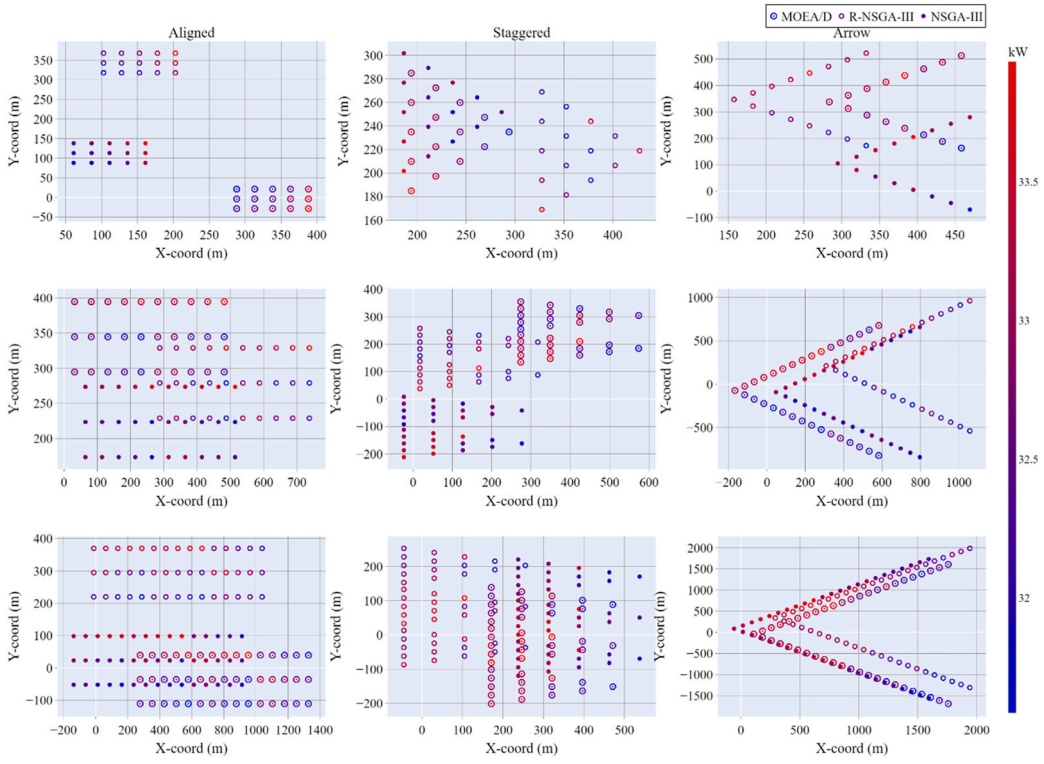

Fig. 17. Layout design of octagonal WEC with 15, 30, and 45 device.

enhanced by positive interaction (LCoE decreased by 4–7 %), whereas the effect of shadowing increased LCoE by almost 62 %. Both the ideal and worst-case scenarios for orientation were modeled, and it is expected that a practical park will have an LCoE somewhere in the middle.

These simulations prove the selection of a 100-kW power rating for the EMnO calculations. The EMnOs' optimum layouts are shown in Figs. 16 and 17 for dividing the parks into aligned, staggered, and arrow arrays. While convergence was reached for results from 15 to 30 W ECs, it may still be a while until convergence of results for WECs parks is achieved due to the computational complexity of these simulations.

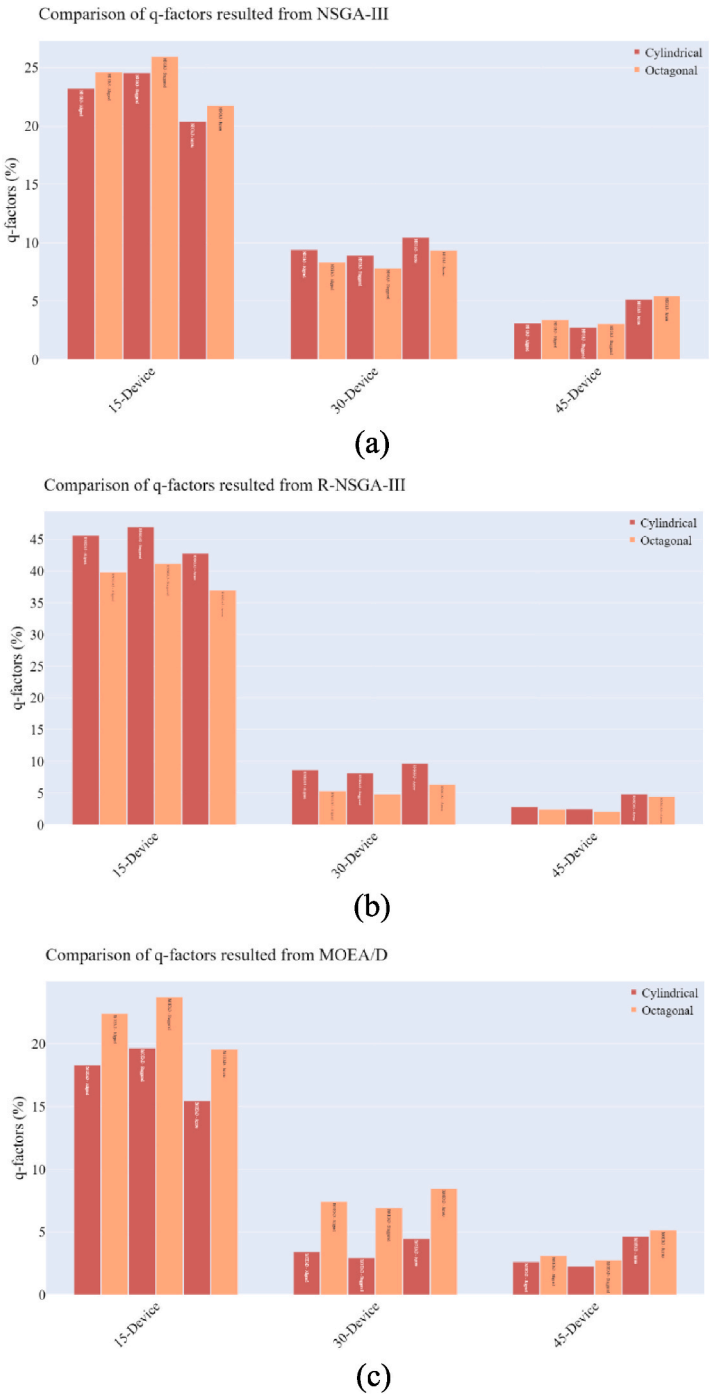

Fig. 18. Comparison of *q*-factor results from (a) NSGA-III, (b) *R*-NSGA-III, and (c) MOEA/D for each layout design in cylindrical and octagonal shapes.

Accordingly, it can be deduced that the best results were obtained for 45 W ECs. The first, second, and third rows display the results for distances of 25, 50, and 75 *m* of interaction, respectively.

Based on the initial layouts in Fig. 11 and mathematical formulation in Section 3, the optimized shape and size of multi-axis WECs in arrays of 15, 30, and 45 buoys were obtained with three different EMnO algorithms. Each algorithm searches for the optimal deployment of each WEC based on the wave energy produced in the domain. The three predefined arrays are clusters that only move towards the domain to be placed at the potential x and y coordinates with a distinct separation distance between each device. In addition, the optimal layouts are defined in terms of arrays with maximum energy production by comparing three EMnO algorithms and three different layout configurations. Figs. 16 and 17 display the outcomes of layout optimization, where the objective is to achieve the constructive q-factor. Compared to 30-buoy arrays, 45-buoy arrays have an optimized q-factor of 3.43 % greater on average. The q-factors grew in two distinct ways in the experiments. The first round of experiments focused on 30 buoys - this array is well-known for offering the absolute maximum in terms of energy output. Each algorithm will search for the optimal deployment of each WECs based on the produced wave energy in the domain. In fact, the three pre-defined arrays are clusters which only move towards the domain to be placed at the potential x and y coordinate with distinct separation distance between each device. Fig. 18 shows the resultant q-factors that are much larger than expected and buoys oscillating with an unrealistically large displacement.

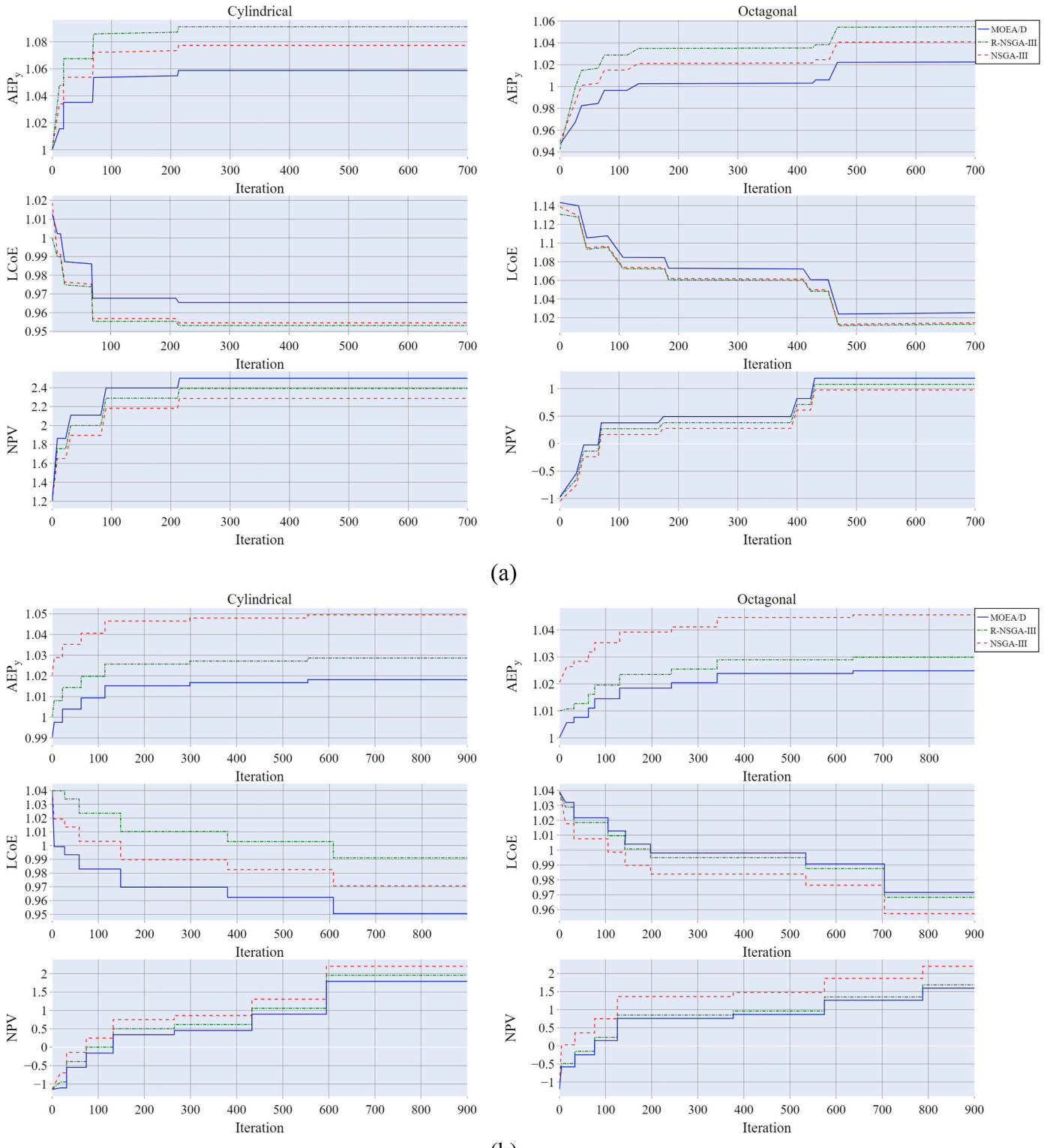

Fig. 19. AEP$_y$, LCoE, and NPV of (a) 15-, (b) 30-, and (c) 45-device layouts.

The optimal configurations, shown in Figs. 16 and 17 include rows of WECs facing the incoming wave field, located far enough apart to prevent hydrodynamic contact when the interaction distance is 50 *m*. These figures display the best layouts for three distinct configurations of cylindrical and octagonal geometries, as well as the annual average power output of the devices. It is clear that the WECs are not affected by shadowing in the regions where the more extensive hydrodynamic interaction is calculated. The complete hydrodynamic coupling amongst all the devices was further calculated. Even if convergence has not been attained in parks with 45 W ECs, the WECs are clustered together to reduce expenditure and tend to line up in rows at 90° to the wave direction. Accordingly, Fig. 19 illustrates the relationship between the

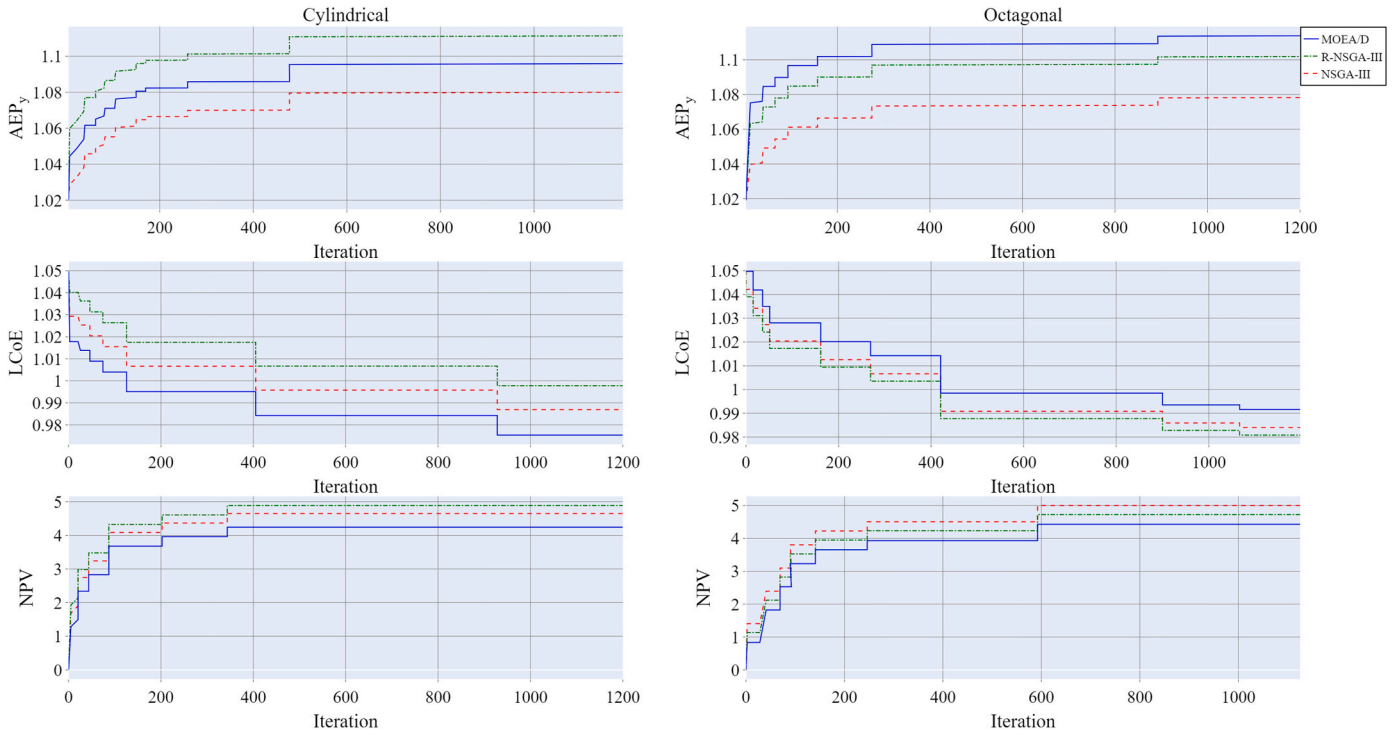

(c)

Fig. 19. (*continued*).

Table 5
Computation time of each optimization framework.

Model	No. Of cores	Run time
NSGA-III + NEMOH	12	≈19.5 h
R-NSGA-III + NEMOH	12	≈17.5 h
MOEA/D + NEMOH	12	≈20.0 h

number of optimization iterations and AEP$_y$, LCoE, and NPV. As anticipated, the LCoE decreases as energy production and NPV rise with iterations. Additionally, the total computation for each optimization framework is presented in Table 5.

The structural dynamic response could also be estimated using RAO, which decelerates when the PTO damping coefficient, b_1, is enhanced. Therefore, determining the best value for the damping coefficient of the PTO mechanism is critical for maximizing the average absorbed power. The averaged wave energy spectrum off the coast of Oman was employed to determine the mean absorbed power for different settings of the PTO mechanism's damping coefficient, as illustrated in Fig. 20. In each damping coefficient value, the mean absorbed power for each frequency element was added to obtain the overall mean absorbed power. Fig. 21 shows that 510 kN/m is the optimal value for the PTO mechanism's damping coefficient, b_1, at the overall maximum mean absorbed power. The ideal damping coefficient of the PTO mechanism was then used to determine the global mean absorbed power of a structural system with the best possible geometric shape off the coast of Oman. To specify the likelihood of the structure occurring off the coast of Oman, its absorbed power matrix was calculated, as shown in Figs. 22 and 23.

The hydrodynamic characteristics for the surge, heave, and pitch motion of the multi-axis WEC are shown in Fig. 24. These include the added mass A_{11}, A_{33}, A_{55}, radiation damping coefficient B_{11}, B_{33}, B_{55}, and wave excitation force, F_{ex1}, F_{ex3}, F_{ex5}. The values are clearly greater for the optimum octagonal configuration than for the cylindrical one. The hydrodynamic characteristics for these three motions also reveal that the moment of added mass is quite underpredicted, while the

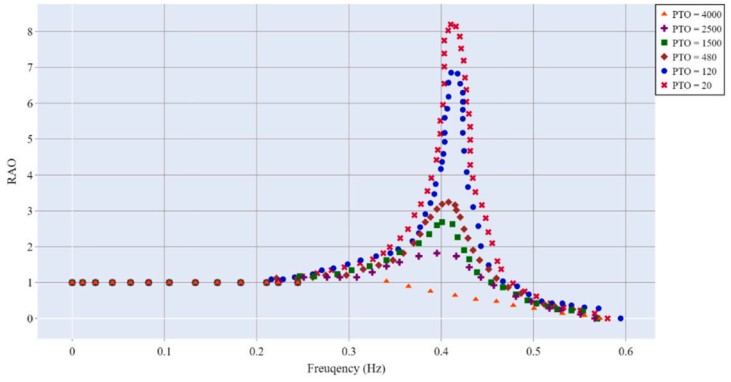

Fig. 20. RAO coefficient of octagonal shape for different PTO settings.

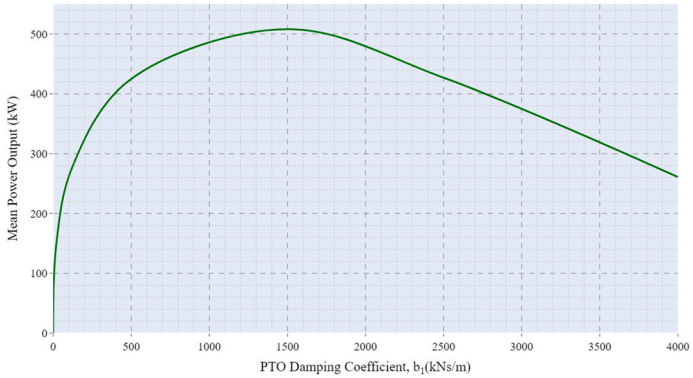

Fig. 21. Variation of mean absorbed power for a range of values of the PTO damping coefficient.

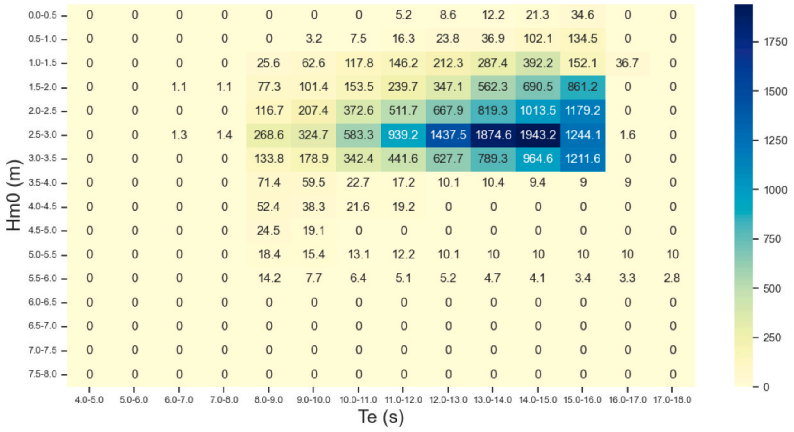

Fig. 22. Matrix showing the average power absorbed (W) by the optimal cylindrical shape from 2018 to 2019.

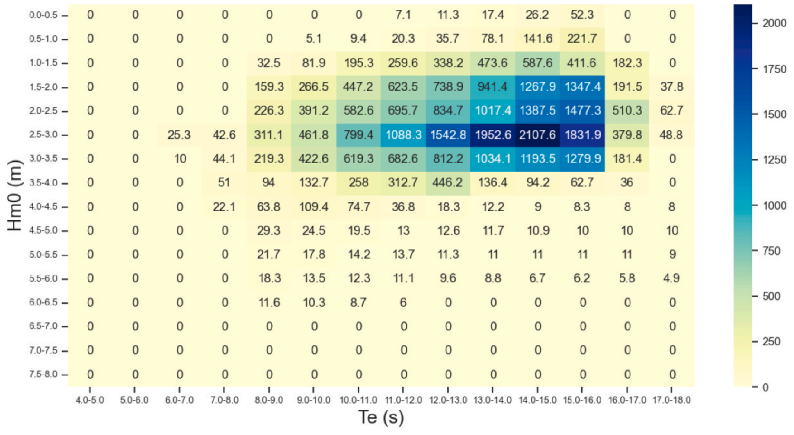

Fig. 23. Matrix showing the average power (W) absorbed by the optimal octagonal shape from 2018 to 2019.

moment of wave excitation is hardly overpredicted. Excluding the cases of incident waves and irregular frequencies, the radiation damping coefficient findings are similar.

Since NEMOH has well-predicted all hydrodynamic parameters, the predictions of RAOs of the multi-axis WEC are in good agreement as expected, as shown in Fig. 25. Except for the magnitudes at the resonance phases for pitch motions, all RAO estimations are similar. Since surge and pitch are intimately integrated, the variations in pitch motion may explain the variations in surge RAOs.

The limitations previously mentioned can have varying degrees of impact on the findings. Computational constraints might lead to less-than-optimal configurations, while the constraints posed by data availability might make the models less adaptable to changing future conditions. Subsequently, algorithmic limitations could question the global optimality of the solutions found. Moreover, the results of this research have multifaceted implications. For industries, it means the potential for cost-effective and efficient wave energy solutions. Accordingly, countries with expansive coastlines might witness a paradigm shift in their energy portfolios, reducing emissions and concurrently advancing towards their climate change commitments and specific sustainable development goals.

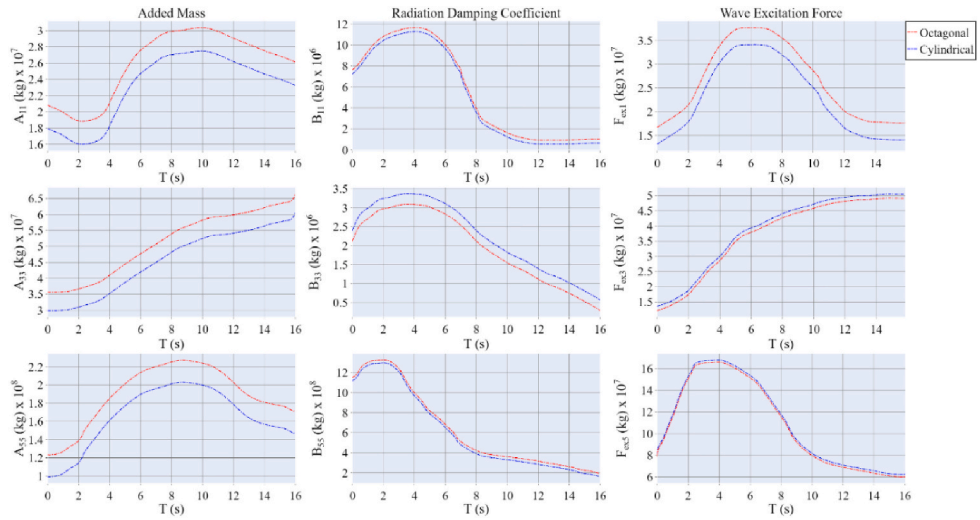

Fig. 24. Added mass, radiation damping coefficient, and wave excitation force of surge, heave, and pitch motions in optimal cylindrical and octagonal shapes.

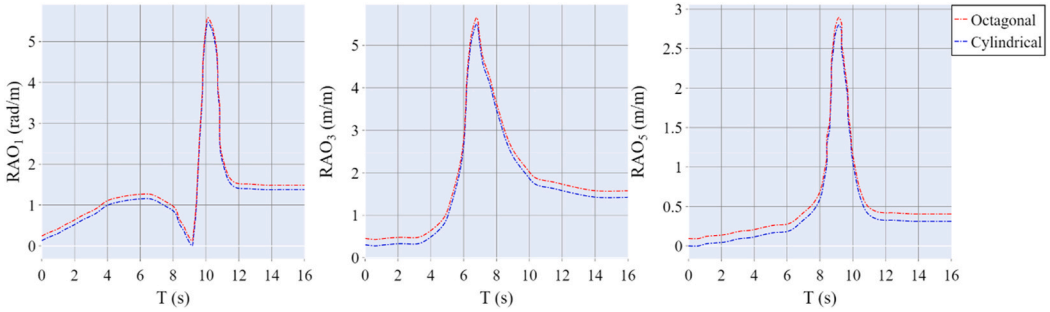

Fig. 25. RAO of the surge, heave, and pitch motions in optimal cylindrical and octagonal shapes.

6. Conclusion

This research proposes three EMnO Optimization frameworks for optimizing the layout, geometry, and economic cost of a multi-axis WEC. Six objective functions were developed, including maximizing absorbed power, minimizing LCoE, NPV, separation distance, and q-factor. Different geometries and dimensions were considered, and hydrodynamic coefficients were obtained using NEMOH. The optimal geometry was then used for layout design with aligned, staggered, and arrow configurations containing 15 to 45 devices.

The coast of Oman was used as a practical example for designing wave farms. Wave energy spectra from 2018 to 2019 were analyzed to determine the optimal geometry and layout of the wave farm. The optimal geometry was found to be octagonal and cylindrical shape with radius of 29 and 26.3 *m*, height of 13.6 and 15.2 *m*, and draft of 16.3 and 17.2 *m*, respectively. The study emphasized the sensitivity of outcomes to various factors in the hydrodynamic model, with hydrodynamic interaction significantly impacting the wave farm design. Adverse interactions and shadowing effects were found to reduce power generation and NPVs. The LCoE value was influenced by electrical system features. Optimization considering different design features and hydrodynamic interactions yielded the best wave farm designs, especially for larger parks with 45 devices. Additionally, increasing the number of WECs led to a decrease in the LCoE of the wave farms. In addition, the optimal damping coefficient of the PTO mechanism was determined to be $b_1 =$ 510 kN/m. The absorbed power matrix for the device at the site was obtained using a method similar to Babarit et al. [76]. The average absorbed power across parameters was estimated to be approximately 392 kW. These findings have important implications for the improvement and advancement of WEC design.

- Optimized performance: This research was able to identify the key parameters and operational conditions that lead to optimal energy conversion efficiency. These findings can guide the design process, with engineers able to prioritize these factors to achieve better performance.
- Cost-efficiency: Our study has shown how particular design choices can lead to cost-effective manufacturing and deployment of WECs. By focusing on these aspects, it will be possible to drive down the cost of wave energy, making it more competitive with other renewable energy sources.
- Scalability: The results of our study can inform the design of scalable WEC systems. With the understanding of how individual converters interact in an array and the environmental factors influencing their performance, designers can better plan for the deployment of larger, more efficient wave farms.

The WEC model was simplified to manage computational demands, potentially causing differences between simulated and actual results. The optimization was based on noisy wave data, prone to errors from outliers and inherent uncertainties. Improving data processing and using adaptive algorithms might refine results and better account for real-world conditions. This study provides foundational insights into multi-axis WEC optimization, but there are still avenues for advancement. Leveraging computational tools may yield more precise outcomes. Incorporating real-time wave data could enhance model adaptability in future research. Furthermore, investigating alternative optimization methods or combined models might offer better and more universally optimal results. Recognizing these constraints will further refine our grasp on WEC optimization.

In summary, this WEC adaptive optimization carries a significant

global impact. It represents a step towards worldwide sustainability by tackling both environmental and economic challenges. As countries strive for their environmental milestones and industries pivot towards eco-friendly solutions, this research underscores the importance of refining wave energy designs. Moving forward, continued advancements in this domain, coupled with supportive policies, could mark a transformative era for renewable energy, steering the world closer to its sustainability targets.

Credit author statement

Alireza Shadmani: Conceptualization, Data Curation, Formal analysis, Investigation, Methodology, Visualization, Writing – Original Draft. Mohammad Reza Nikoo: Conceptualization, Methodology, Resources, Supervision, Writing – Review & Editing. Amir H. Gandomi: Conceptualization, Resources, Supervision, Writing – Review & Editing.

Declaration of competing interest

The authors declare that they have no known competing financial interests or personal relationships that could have appeared to influence the work reported in this paper.

Data availability

Data will be made available on request.

Acknowledgements

Authors declare that no funding was provided for this research.

References

[1] Jin S, Greaves D. Wave energy in the UK: status review and future perspectives. Renew Sustain Energy Rev 2021;143:110932. https://doi.org/10.1016/j.rser.2021.110932.
[2] Guo B, Ringwood JV. A review of wave energy technology from a research and commercial perspective. IET Renew Power Gener 2021;15(14):3065–90. https://doi.org/10.1049/RPG2.12302.
[3] Clemente D, Rosa-Santos P, Taveira-Pinto F. On the potential synergies and applications of wave energy converters: a review. Renew Sustain Energy Rev 2021;135:110162.
[4] Europe must choose a green future," Energy Transition, Apr. 24, 2018.
[5] Kurnia R, Ducrozet G. NEMOH V3. 0 user manual. Ecole Cent. Nantes; 2022.
[6] Lee CH, Newman JN. Wamit user manual, vol. 42. WAMIT Inc; 2006.
[7] Babarit A, Delhommeau G. Theoretical and numerical aspects of the open source BEM solver NEMOH. 2015.
[8] McNatt JC, Venugopal V, Forehand D. A novel method for deriving the diffraction transfer matrix and its application to multi-body interactions in water waves. Ocean Eng 2015;94:173–85. https://doi.org/10.1016/J.OCEANENG.2014.11.029.
[9] Reikard G, Robertson B, Bidlot JR. Wave energy worldwide: simulating wave farms, forecasting, and calculating reserves. Int. J. Mar. Energy 2017;17:156–85. https://doi.org/10.1016/J.IJOME.2017.01.004.
[10] Penalba M, Kelly T, Ringwood J. Using NEMOH for modelling wave energy converters: a comparative study with WAMIT. 2017.
[11] Sheng W, Tapoglou E, Ma X, Taylor CJ, Dorrell RM. Hydrodynamic studies of floating structures: comparison of wave-structure interaction modelling. Ocean Eng 2022;249:110878.
[12] Babarit A. Impact of long separating distances on the energy production of two interacting wave energy converters. Ocean Eng 2010;37(8–9):718–29. https://doi.org/10.1016/J.OCEANENG.2010.02.002.
[13] Marchesi E, Negri M, Malavasi S. Development and analysis of a numerical model for a two-oscillating-body wave energy converter in shallow water. Ocean Eng 2020;214:107765. https://doi.org/10.1016/J.OCEANENG.2020.107765.
[14] Bozzi S, Giassi M, Miquel AM, Antonini A, Bizzozero F. Wave energy farm design in real wave climates: the Italian offshore. Energy 2017;122:378–89. https://doi.org/10.1016/J.ENERGY.2017.01.094.
[15] Verao Fernandez G, Stratigaki V, Troch P. Irregular wave validation of a coupling methodology for numerical modelling of near and far field effects of wave energy converter arrays. Energies 2019;12(3):538.
[16] Verao Fernandez G, Balitsky P, Stratigaki V, Troch P. Coupling methodology for studying the far field effects of wave energy converter arrays over a varying bathymetry. Energies 2018;11(11):2899.
[17] Silva D, Rusu E, Soares CG. Evaluation of various technologies for wave energy conversion in the Portuguese nearshore. At Energ 2013;6:1344–64. https://doi.org/10.3390/EN6031344. vol. 6, no. 3, pp. 1344–1364, Mar. 2013.
[18] Teixeira-Duarte F, Clemente D, Giannini G, Rosa-Santos P, Taveira-Pinto F. Review on layout optimization strategies of offshore parks for wave energy converters. Renew Sustain Energy Rev 2022;163:112513.
[19] Yang B, Wu S, Zhang H, Liu B, Shu H, Shan J, Ren Y, Yao W. Wave energy converter array layout optimization: a critical and comprehensive overview. Renew Sustain Energy Rev 2022;167:112668.
[20] Göteman M, Giassi M, Engström J, Isberg J. Advances and challenges in wave energy park optimization—a review. Front Energy Res 2020;8. https://doi.org/10.3389/FENRG.2020.00026/FULL.
[21] Loukogeorgaki E, Michailides C, Lavidas G, Chatjigeorgiou IK. Layout optimization of heaving Wave Energy Converters linear arrays in front of a vertical wall. Renew Energy 2021;179:189–203.
[22] Lyu J, Abdelkhalik O, Gauchia L. Optimization of dimensions and layout of an array of wave energy converters. Ocean Eng 2019;192:106543.
[23] Budal K. Theory for absorption of wave power by a system of interacting bodies. J Ship Res 1977;21(4):248–54.
[24] Mercadé Ruiz P, Nava V, Topper MBR, Minguela PR, Ferri F, Kofoed JP. Layout optimisation of wave energy converter arrays. At Energ 2017;10. https://doi.org/10.3390/EN10091262. vol. 10, no. 9, p. 1262, Aug. 2017.
[25] Sarkar D, Contal E, Vayatis N, Dias F. Prediction and optimization of wave energy converter arrays using a machine learning approach. Renew Energy 2016;97:504–17.
[26] Shadmani A, Reza Nikoo M, Etri T, Gandomi AH. A multi-objective approach for location and layout optimization of wave energy converters. Appl Energy 2023;347:121397. https://doi.org/10.1016/j.apenergy.2023.121397.
[27] Sharp C, DuPont B. A multi-objective real-coded genetic algorithm method for wave energy converter array optimization. In: International conference on offshore mechanics and arctic engineering. American Society of Mechanical Engineers; 2016. V006T09A027.
[28] Abdulkadir H, Abdelkhalik O. Optimization of heterogeneous arrays of wave energy converters. Ocean Eng 2023;272:113818.
[29] Goggins J, Finnegan W. Shape optimisation of floating wave energy converters for a specified wave energy spectrum. Renew Energy 2014;71:208–20.
[30] McCabe AP. Constrained optimization of the shape of a wave energy collector by genetic algorithm. Renew Energy 2013;51:274–84. https://doi.org/10.1016/J.RENENE.2012.09.054.
[31] Bouali B, Larbi S. Sequential optimization and performance prediction of an oscillating water column wave energy converter. Ocean Eng 2017;131:162–73.
[32] Poguluri SK, Kim D, Lee Y, Shin J-H, Bae YH. Design optimization of asymmetric wave energy converter using artificial neural network model. Int J Nav Archit Ocean Eng 2023;15:100529.
[33] Ding H, Zang J, Jin P, Ning D, Zhao X, Liu Y, Blenkinsopp Ch, Chen Q. Optimization of the hydrodynamic performance of a wave energy converter in an integrated cylindrical wave energy converter-type breakwater system. J Offshore Mech Arctic Eng 2023;145(5):054501.
[34] Shadman M, Estefen SF, Rodriguez CA, Nogueira ICM. A geometrical optimization method applied to a heaving point absorber wave energy converter. Renew Energy 2018;115:533–46. https://doi.org/10.1016/j.renene.2017.08.055.
[35] Guo B, V Ringwood J. Geometric optimisation of wave energy conversion devices: a survey. Appl Energy 2021;297:117100.
[36] Shadmani A, Nikoo MR, Al-Raoush RI, Alamdari N, Gandomi AH. The optimal configuration of wave energy conversions respective to the nearshore wave energy potential. Energies 2022;15(20):7734.
[37] Garcia-Teruel A, DuPont B, Forehand DIM. Hull geometry optimisation of wave energy converters: on the choice of the optimisation algorithm and the geometry definition. Appl Energy 2020;280:115952. https://doi.org/10.1016/J.APENERGY.2020.115952.
[38] Birk L. Application of constrained multi-objective optimization to the design of offshore structure hulls. J Offshore Mech Arctic Eng 2009;131(1):1–9. https://doi.org/10.1115/1.2957919/456353.
[39] Kurniawan A, Moan T. Multi-objective optimization oa wave energy absorber geometry. In: Proceeding of 27th international workshop on water waves and floating bodies, copenhagen; 2012. p. 22–5.
[40] Alamian R, Shafaghat R, Safaei MR. Multi-objective optimization of a pitch point absorber wave energy converter. Water 2019;11(5):969.
[41] Neary VS, Kobos PH, Jenne DS, Yu Y-H. Levelized cost of energy for marine energy conversion (mec) technologies. Albuquerque, NM (United States): Sandia National Lab.(SNL-NM); 2016.
[42] Chozas J. International levelised cost of energy for ocean energy technologies. Ocean Energy Syst; 2015.
[43] Curto D, Favuzza S, Franzitta V, Musca R, Navarro Navia MA, Zizzo G. Evaluation of the optimal renewable electricity mix for Lampedusa island: the adoption of a technical and economical methodology. J Clean Prod 2020;263:121404. https://doi.org/10.1016/J.JCLEPRO.2020.121404.
[44] Piscopo V, Benassai G, Della Morte R, Scamardella A. Cost-based design and selection of point absorber devices for the mediterranean sea. Energies 2018;11(4):946.
[45] Macadré L-M, McAuliffe F, Keysan O, Donovan M, Armstrong S, Murphy J, Lynch K. Optimal power aggregation methods for marine renewable energy converters; a combined economic and reliability approach. In: Proceedings of the 11th European wave and tidal energy conference. (EWTEC)(Nantes); 2015.
[46] Kotb ATM, Nawar MAA, Attai YA, Mohamed MH. Performance optimization of a modified Wells turbine for wave energy conversion. Ocean Eng 2023;280:114849. https://doi.org/10.1016/j.oceaneng.2023.114849.

[47] Saveca J, Sun Y, Wang Z. Machine learning and particle swarm inspired success history based adaptive multi-objective differential evolution for optimization of heaving buoy point absorber. Ocean Eng 2023;284:115189.
[48] Lin W, Shanab BH, Lenderink C, Zuo L. Multi-objective optimization of the buoy shape of an ocean wave energy converter using neural network and genetic algorithm. 2nd Model. Estim. Control Conf. MECC 2022;55(37):145–50. https://doi.org/10.1016/j.ifacol.2022.11.175. Jan. 2022.
[49] Tournant P, Perret G, Smaoui H, Sergent P, Marin F. Shape parameters optimisation of a quayside heaving rectangular wave energy converter. Appl Energy 2023;343:121232. https://doi.org/10.1016/j.apenergy.2023.121232.
[50] Garcia-Teruel A, Forehand DIM. Manufacturability considerations in design optimisation of wave energy converters. Renew Energy 2022;187:857–73. https://doi.org/10.1016/j.renene.2021.12.145.
[51] Jia H, Pei Z, Tang Z, Yang J. Modeling and analysis of an inertia wave energy converter and its optimal design. J Mar Sci Eng 2023;11(7). https://doi.org/10.3390/jmse11071351.
[52] Ancellin M, Dias F. Capytaine: a Python-based linear potential flow solver. J Open Source Softw 2019;4(36):1341. https://doi.org/10.21105/JOSS.01341.
[53] Blank J, Deb K. Pymoo: multi-objective optimization in python. IEEE Access 2020;8:89497–509.
[54] Fortin F-A, De Rainville F-M, Gardner M-AG, Parizeau M, Gagné C. DEAP: evolutionary algorithms made easy. J Mach Learn Res 2012;13(1):2171–5.
[55] Giassi M, Castellucci V, Göteman M. Economical layout optimization of wave energy parks clustered in electrical subsystems. Appl Ocean Res 2020;101:102274.
[56] Veigas M, López M, Iglesias G. Assessing the optimal location for a shoreline wave energy converter. Appl Energy 2014;132:404–11.
[57] Delmonte N, Robles E, Cova P, Giuliani F, Fay FX, Lopez J, Ruol P, Martinelli L. An iterative refining approach to design the control of wave energy converters with numerical modeling and scaled HIL testing. Energies 2020;13(10). https://doi.org/10.3390/en13102508.
[58] Wuillaume PY. Study of the free surface Green function at zero forward speed in finite water depth using Newman's method. Appl Ocean Res 2022;120. https://doi.org/10.1016/j.apor.2021.103036.
[59] Zhu Y. A global approximation to the Green function for diffraction radiation of water waves. Eur. J. Mech. - BFluids 2017;65:54–64. https://doi.org/10.1016/J.EUROMECHFLU.2017.02.008.
[60] Wang Y, Yang J, Hu Z, Xiao L. Theoretical research on hydrodynamics of a geometric spar in frequency-and time-domains. J Hydrodyn 2008;20(1):30–8. https://doi.org/10.1016/S1001-6058(08)60024-4.
[61] Sheng W. Wave energy conversion and hydrodynamics modelling technologies: a review. Renew Sustain Energy Rev 2019;109:482–98. https://doi.org/10.1016/J.RSER.2019.04.030.
[62] Aggidis GA, Taylor CJ. Overview of wave energy converter devices and the development of a new multi-axis laboratory prototype. IFAC-PapersOnLine 2017;50(1):15651–6.
[63] Zhang Z, Lei Z, Jin T, Li J, Todo Y, Gao S. A new sight to optimize the layout of wave energy converters. In: 2023 4th international conference on computer engineering and application (ICCEA); 2023. p. 258–63. https://doi.org/10.1109/ICCEA58433.2023.10135364.
[64] Han M, Cao F, Shi H, Zhu K, Dong X, Li D. Layout optimisation of the two-body heaving wave energy converter array. Renew Energy 2023;205:410–31. https://doi.org/10.1016/j.renene.2023.01.100.
[65] Rajagopalan R. A multi-objective optimization approach for data fusion in mobile agent based distributed sensor networks. In: 2010 IEEE instrumentation & measurement technology conference proceedings, IEEE; 2010. p. 208–12.
[66] Deb K, Jain H. An evolutionary many-objective optimization algorithm using reference-point-based nondominated sorting approach, part I: solving problems with box constraints. IEEE Trans Evol Comput 2013;18(4):577–601.
[67] Özdemir S, Attea BA, Khalil ÖA. Multi-objective clustered-based routing with coverage control in wireless sensor networks. Soft Comput 2013;17(9):1573–84.
[68] Deb K, Pratap A, Agarwal S, Meyarivan T. A fast and elitist multiobjective genetic algorithm: nsga-II. IEEE Trans Evol Comput 2002;6(2):182–97.
[69] Srinivas N, Deb K. Muiltiobjective optimization using nondominated sorting in genetic algorithms. Evol Comput 1994;2(3):221–48.
[70] Kumar H, Yadav SP. NSGA-II based fuzzy multi-objective reliability analysis. Int. J. Syst. Assur. Eng. Manag. 2017;8(4):817–25.
[71] Vesikar Y, Deb K, Blank J. Reference point based NSGA-III for preferred solutions. In: 2018 IEEE symposium series on computational intelligence (SSCI). IEEE; 2018. p. 1587–94.
[72] Zhang Q, Li H. MOEA/D: a multiobjective evolutionary algorithm based on decomposition. IEEE Trans Evol Comput 2007;11(6):712–31.
[73] Yetgin H, Cheung KTK, Hanzo L. Multi-objective routing optimization using evolutionary algorithms. In: 2012 IEEE wireless communications and networking conference (WCNC), IEEE; 2012. p. 3030–4.
[74] Zhou Q. PyMesh—geometry processing library for Python," *softw*. Available Download Httpsgithub ComPyMeshPyMesh; 2019.
[75] Jain H, Deb K. An evolutionary many-objective optimization algorithm using reference-point based nondominated sorting approach, part II: handling constraints and extending to an adaptive approach. IEEE Trans Evol Comput 2013;18(4):602–22.
[76] Babarit A, Clement AH. Shape optimisation of the searev wave energy converter. Proceeding of World Renewable Energy Conference; 2006.